


2014

Propagation Prediction Over Random Rough Surface By Zeroth Order Induced Current Density

Narayana Srinivasan Balu
University of Massachusetts Amherst

Follow this and additional works at: https://scholarworks.umass.edu/masters_theses_2

 Part of the [Electromagnetics and Photonics Commons](#), [Other Electrical and Computer Engineering Commons](#), [Signal Processing Commons](#), and the [Systems and Communications Commons](#)

Recommended Citation

Balu, Narayana Srinivasan, "Propagation Prediction Over Random Rough Surface By Zeroth Order Induced Current Density" (2014). *Masters Theses*. 129.
https://scholarworks.umass.edu/masters_theses_2/129

This Open Access Thesis is brought to you for free and open access by the Dissertations and Theses at ScholarWorks@UMass Amherst. It has been accepted for inclusion in Masters Theses by an authorized administrator of ScholarWorks@UMass Amherst. For more information, please contact scholarworks@library.umass.edu.

**PROPAGATION PREDICTION OVER RANDOM ROUGH
SURFACE BY ZEROth ORDER INDUCED CURRENT DENSITY**

A Thesis Presented

by

NARAYANA SRINIVASAN BALU

Submitted to the Graduate School of the
University of Massachusetts Amherst in partial fulfillment
of the requirements for the degree of

MASTER OF SCIENCE IN ELECTRICAL AND COMPUTER ENGINEERING

SEPTEMBER 2014

Electrical and Computer Engineering

© Copyright by Narayana Srinivasan Balu 2014
All Rights Reserved

**PROPAGATION PREDICTION OVER RANDOM ROUGH
SURFACE BY ZEROth ORDER INDUCED CURRENT DENSITY**

A Thesis Presented

by

NARAYANA SRINIVASAN BALU

Approved as to style and content by:

Ramakrishna Janaswamy, Co-Chair

Do-Hoon Kwon, Co-Chair

Stephen Frasier, Member

Christopher V.Hollot, Department Chair
Electrical and Computer Engineering

*To my Mother, Kalaiarasi and my Father, Balu.
Matha, Pitha, Guru, Deivam.*

ACKNOWLEDGMENTS

I would like to express my finest gratitude to my advisor Prof. Ramakrishna Janaswamy for his constant guidance, support and motivation. It was truly a rewarding experience working with him and I thank him for helping me in this work. This thesis has helped me take a big step towards building a structured thought process and efficient organization of work. I thank Prof. Do-Hoon Kwon for his support in this work and Prof. Stephen Frasier for his valuable suggestions. I am grateful to my family for always being there for me and providing moral support during testing times. I also wish to thank my friend Selman, who was always enthusiastic to spend time during brainstorming sessions and helping me out during the initial days of this work. A special thanks to all the members of Antennas and Propagation Laboratory for making this journey enjoyable.

ABSTRACT

PROPAGATION PREDICTION OVER RANDOM ROUGH SURFACE BY ZEROth ORDER INDUCED CURRENT DENSITY

SEPTEMBER 2014

NARAYANA SRINIVASAN BALU

B.Tech., NATIONAL INSTITUTE OF TECHNOLOGY, TRICHY, INDIA

M.S.E.C.E., UNIVERSITY OF MASSACHUSETTS AMHERST

Directed by: Professor Ramakrishna Janaswamy

Electromagnetic wave propagation over random sea surfaces is a classical problem of interest for the Navy, and significant research has been done over the years. Here we make use of numerical and analytical methods to predict the propagation of microwaves over random rough surface. The numerical approach involves utilization of the direct solution (using Volterra integral equation of the second kind) to currents induced on a rough surface due to forward propagating waves to compute the scattered field. The mean scattered field is computed using the Monte-Carlo method. Since the exact solution (consisting of an infinite series) to induced current density is computationally intensive, there exists a need to predict the propagation using the closely accurate zeroth order induced current (first term of the series) for time-varying multiple realizations of a random rough surface in a computationally efficient manner. The wind-speed dependent, fully-developed, Pierson-Moskowitz sea spectrum has been considered in order to model a rough sea surface, although other partially-developed roughness spectra may also be utilized. An analytical solution based on the zeroth order current density obtained by deriving the mean scattered field as a function of the range and vertical height by directly using the Parabolic Equation (PE) approximation method and the resulting Green's function has been utilized for a comparative study. The analytical solution takes into account the diffused component of the scattered field.

TABLE OF CONTENTS

	Page
ACKNOWLEDGMENTS	v
ABSTRACT	vi
LIST OF TABLES.....	viii
LIST OF FIGURES.....	ix
 CHAPTER	
1. INTRODUCTION	1
1.1. Background and Motivation	1
1.2. Overview	2
2. RANDOM ROUGH SURFACE.....	4
2.1. Rough Surface as a Random Process	4
3. INDUCED CURRENT DENSITY	10
3.1. Direct & Exact Solution	10
3.2. Zeroth Order Solution	13
4. PROPAGATION FACTOR.....	16
4.1. Scattered field along a vertical line.....	16
4.2. Zeroth Order Asymptotic Expression	21
5. ZEROth ORDER SOLUTION IN HIGHER FREQUENCY BANDS AND WIND SPEEDS.....	26
5.1. Mean Signal PF using Monte-Carlo simulations.....	26
5.2. Mean Power PF using Monte-Carlo simulations.....	41
5.3. Asymptotic Zeroth Order Solution	54
6. SUMMARY AND CONCLUSIONS.....	58
BIBLIOGRAPHY.....	61

LIST OF TABLES

Table	Page
Table 1: Monte Carlo Mean Signal PF at different frequencies and roughness at $X_{max} = 450\text{m}$	37

LIST OF FIGURES

Figure	Page
1: PM Spectrum for varying wind speeds.....	5
2: Correlation function for the PM spectrum for varying wind speeds	6
3: Single realization of random rough sea surface using Gaussian height statistics & PM spectrum, $U=10\text{m/s}$, $\sigma_h=0.53\text{m}$, $\rho_c=25.6\text{m}$, $N_p=512$, $\Delta x=0.88\text{m}$	8
4: Random rough surfaces at varying wind speeds	9
5: Comparison of absolute J^{num} and J^0 for a wind-generated PM random rough surface at 1 GHz, $\lambda =0.3\text{m}$, $H_f=3\text{m}$, $U=10\text{m/s}$, $\sigma_h=0.53\text{m}$, $\rho_c=25.6\text{m}$, $N_p=512$, $\Delta x=0.88\text{m}$, $\sigma_z=4\lambda/3$, max. absolute slope $\alpha_g=0.14$	14
6: Phase (degrees) of J^{num} and J^0 for a wind-generated PM random rough surface at 1 GHz, $\lambda =0.3\text{m}$, $H_f=3\text{m}$, $U=10\text{m/s}$, $\sigma_h=0.53\text{m}$, $\rho_c=25.6\text{m}$, $N_p=512$, $\Delta x=0.88\text{m}$, $\sigma_z=4\lambda/3$, max. absolute slope $\alpha_g=0.14$	15
7: PF for a single realization of a PM surface	18
8: Mean PF for 400 realizations of PM surface	19
9: Schematic depicting the specular reflection and direct incidence.....	20
10: Comparison of Mean PF for 400 surface realizations, $\lambda =0.3\text{m}$, $H_f=3\text{m}$, $U=10\text{m/s}$, $\sigma_h=0.53\text{m}$, $\rho_c=25.6\text{m}$, $N_p=512$, $\Delta x=0.88\text{m}$, $\sigma_z=4\lambda/3$, max. absolute slope $\alpha_g=0.14$	24
11: Monte-Carlo mean signal PF of 400 surface realizations at 1 GHz,	27
12: Monte-Carlo mean signal PF of 400 surface realizations at 1 GHz,	28
13: Monte-Carlo mean signal PF of 400 surface realizations at 1 GHz,	28
14: Monte-Carlo mean signal PF of 400 surface realizations at 1 GHz,	29
15: Monte-Carlo mean signal PF of 400 surface realizations at 3 GHz,	29
16: Monte-Carlo mean signal PF of 400 surface realizations at 3 GHz,	30
17: Monte-Carlo mean signal PF of 400 surface realizations at 3 GHz,	30
18: Monte-Carlo mean signal PF of 400 surface realizations at 3 GHz,	31
19: Monte-Carlo mean signal PF of 400 surface realizations at 5 GHz,	31

20: Monte-Carlo mean signal PF of 400 surface realizations at 5 GHz,	32
21: Monte-Carlo mean signal PF of 400 surface realizations at 5 GHz,	32
22: Monte-Carlo mean signal PF of 400 surface realizations at 5 GHz,	33
23: Monte-Carlo mean signal PF of 400 surface realizations at 10 GHz,	33
24: Monte-Carlo mean signal PF of 400 surface realizations at 10 GHz,	34
25: Monte-Carlo mean signal PF of 400 surface realizations at 10 GHz,	34
26: Monte-Carlo mean signal PF of 600 surface realizations at 10 GHz,	35
27: Monte-Carlo mean signal PF of 400 surface realizations at 10 GHz,	35
28: Monte-Carlo mean signal PF of 600 surface realizations at 10 GHz,	36
29: Phase of integrand for J0 solution w.r.t. integration variable at x=111.8m	38
30: Phase of integrand for J0 solution w.r.t. integration variable at x=450m.....	38
31: Overlay of surface with Jnum and J0 at 10 GHz, 5m/s	39
32: Overlay of surface with Jnum and J0 at 10 GHz, 10m/s	39
33: Overlay of surface with Phase of Jnum and J0 at 10 GHz, 5m/s	40
34: Overlay of surface with Phase of Jnum and J0 at 10 GHz, 10m/s	40
35: Schematic depicting the propagation of radio-waves and angle of incidence, reflection according to Beckmann	42
36: Comparison of mean scattered power from Jnum, J0 of Monte-Carlo with Kirchhoff's solution outlined in Beckmann.....	43
37: Monte-Carlo mean power PF of 400 surface realizations at 1 GHz,.....	44
38: Monte-Carlo mean power PF of 400 surface realizations at 1 GHz,.....	45
39: Monte-Carlo mean power PF of 400 surface realizations at 1 GHz,.....	45
40: Monte-Carlo mean power PF of 400 surface realizations at 1 GHz,.....	46
41: Monte-Carlo mean power PF of 400 surface realizations at 3 GHz,.....	46

42: Monte-Carlo mean power PF of 400 surface realizations at 3 GHz,.....	47
43: Monte-Carlo mean power PF of 400 surface realizations at 3 GHz,.....	47
44: Monte-Carlo mean power PF of 400 surface realizations at 3 GHz,.....	48
45: Monte-Carlo mean power PF of 400 surface realizations at 5 GHz,.....	48
46: Monte-Carlo mean power PF of 400 surface realizations at 5 GHz,.....	49
47: Monte-Carlo mean power PF of 400 surface realizations at 5 GHz,.....	49
48: Monte-Carlo mean power PF of 400 surface realizations at 5 GHz,.....	50
49: Monte-Carlo mean power PF of 400 surface realizations at 10 GHz,.....	50
50: Monte-Carlo mean power PF of 400 surface realizations at 10 GHz,.....	51
51: Monte-Carlo mean power PF of 400 surface realizations at 10 GHz,.....	51
52: Monte-Carlo mean power PF of 400 surface realizations at 10 GHz,.....	52
53: Monte-Carlo mean power PF of 400 surface realizations at 10 GHz,.....	52
54: Monte-Carlo mean power PF of 400 surface realizations at 10 GHz,.....	53
55: Comparison with asymptotic zeroth order at 1 GHz, $\lambda=0.3\text{m}$, $H_f=3\text{m}$, $U=15\text{m/s}$, $\sigma_h=1.19\text{m}$, $\rho_c=57.73\text{m}$, $N_p=512$, $\Delta x=0.88\text{m}$, $X_{max}=450\text{m}$	54
56: Diffused component of asymptotic zeroth order solution at 1 GHz, 15m/s	55
57: Comparison with asymptotic zeroth order at 3 GHz, $\lambda=0.1\text{m}$, $H_f=3\text{m}$, $U=15\text{m/s}$, $\sigma_h=1.19\text{m}$, $\rho_c=57.73\text{m}$, $N_p=512$, $\Delta x=0.88\text{m}$, $X_{max}=450\text{m}$	55
58: Diffused component of asymptotic zeroth order solution at 3 GHz, 15m/s	56
59: Diffused component of asymptotic zeroth order solution at 5 GHz, 15m/s	56
60: Comparison of asymptotic zeroth order solution	57

CHAPTER 1

INTRODUCTION

1.1. Background and Motivation

Radiowave propagation over rough surfaces has been a problem of interest since the 19th century when Lord Rayleigh studied the scattering of sound waves from sinusoidal surfaces ^[1]. The real progress was motivated by its applications in military with the inventions of radar and underwater sonar in the mid-20th century. The problem is of special interest to the Navy in ship to ship communication and radar detection of low-flying targets over the sea surface. In order to reliably predict the radar coverage within an ocean environment, one must accurately account for the effects of the wind-driven ocean roughness on radar propagation. The ability to predict the interaction of fields with rough surfaces has significant impacts on applications like remote sensing, oceanography, communications, material science and optics.

A number of methods like the physical optics, small perturbation, integral equation, modal analysis etc. have been employed to study the scattering and propagation over rough surfaces. Each has its own advantages in specific situations, but the complex time-varying surface profile poses a challenge in computing the scattered field in an efficient manner. The exact solution is interpreted in the sense that no matrix inversion techniques are used and for example, an infinite series solution to the scattering from a PEC sphere is considered exact.

The Monte Carlo method ^{[2][3]} is employed to average the scattered fields due to individual surfaces over an ensemble of realizations. Scattered fields are computed for each surface, and then combined to yield an average scattering cross section or amplitude. As the ensemble size increases, the results converge to a desired statistical moment. Studies have examined the convergence of the Monte Carlo method as a

function of the number of realizations ^[4], as well as the possibility of neglecting unlikely but important surface features due to a finite number of realizations ^[5]. With the Monte Carlo method, there is a lower limit on the length of each surface realization relative to the correlation length of the rough surface. Ten correlation lengths is a common prescription ^[6]. Shorter lengths can yield acceptable results with more surface realizations; although multiple interactions between long-wavelength components may be neglected.

1.2. Overview

In this work we model a rough surface which is a statistical surface with gently varying slopes (with small slope angles). Propagation over this surface is primarily governed by the forward traveling waves that make small angles with respect to the mean surface. In this case, a Parabolic Equation (PE) method, which is an approximation of the Helmholtz equation, is employed. In the PE method, it is assumed that paraxial waves travel in a unidirectional manner in the range coordinate. The resulting Green's function from the PE method is used to derive a new Volterra integral equation of the second kind ^[7]. The induced currents on the rough surface are calculated using this integral equation assuming perfectly conducting (PEC) rough surface and horizontal polarization.

Chapter 2 presents the necessary theoretical background and method to model a statistical 1-D rough surface in order to compute the induced surface current and the scattered field resulting from the current. It describes the signal processing and probability concepts required to model the rough surface. Chapter 3 briefly explains the formulation of the integral equation for the exact solution to current density and the integral for zeroth order current density ^[7].

Chapter 4 contains the derivation of the expression that solve for the scattered field along a vertical line ^[8] for a given maximum horizontal range where the receiver would be located. The chapter contains the procedure wherein, the induced current and rough surface would be segmented into small discrete parts and a linear approximation would be applied to the segmented parts to solve for an integral equation. The analytical expressions to solve for the zeroth order asymptotic propagation factor would be

presented in Chapter 5, wherein, an expression for the non-specular, diffused scattered field based on the zeroth order induced current has been formulated.

A comparison of the zeroth order solutions with the exact solution ^[7], Miller-Brown ^[9], Ament ^[10] and asymptotic expression ^[11] gives us an idea of the validity of zeroth order solution. Also, a comparison of the propagation factors for varying surface roughness (i.e. wind-speed), frequency of incident wave and horizontal range will be analyzed and presented.

CHAPTER 2

RANDOM ROUGH SURFACE

This chapter describes the method for modeling a rough surface as a random process using basic signal processing concepts and statistical theory. Rough surfaces can be either deterministic, as in the case of an irregular land terrain, where the surface profile is approximately a constant with respect to time and can be expressed as an analytical function or statistical, as in case of sea surface which exhibits a complex time varying random surface profile. It is crucial to model the rough surface accurately in order to account for the incidence and scattering at every sampling interval of the surface. When the normal distances of the transmitter and the receiver points relative to the mean surface is a small fraction of the separation distance between the source and observation points, the rough surface is gently varying and the electromagnetic propagation is primarily governed by the forward travelling waves that make small grazing angles with respect to the mean surface.

2.1. Rough Surface as a Random Process

We consider time-harmonic propagation of 2-D microwaves over a one dimensional random rough surface. For simplicity in boundary condition, the surface is considered to be a PEC (Perfect Electric Conductor), although a similar formulation can be done for a finite impedance surface. The typical conductivity of ocean water is around 4.8 S/m at 20° C and acts nearly like a PEC for our analysis, particularly when the grazing angles are small.

A random process, in its simplest term is a collection of time varying random variables which take on a set of possible values associated with a probability density function. A 1-D random rough surface can be treated as a random process, which at a given instant of time depends on the horizontal range x in meters. The random rough surface can be obtained by specifying two functions that define a random process: the power spectral density function (psd) that characterizes the roughness spectrum and the probability

density function (pdf) for the height statistics. The psd defines the correlation between adjacent points on the surface since the auto-correlation function can be obtained by the inverse Fourier transform of the psd. The pdf determines the variation in the amplitude levels of the rough surface.

In our case, we consider the psd to be Pierson-Moskowitz spectrum (PM spectrum), where the root mean square (RMS) surface height σ_h depends on the wind speed U blowing at a height of 19.5m over the mean sea surface. We also consider the pdf of the random variables to be Gaussian distributed with zero mean ($\mu=0$) and standard deviation σ_h .

The PM spectrum is defined as follows^[12]:

$$W(k) = \frac{\alpha}{4|k|^3} e^{-3\kappa_p^2/2k^2} \quad \text{Eq. 2.1.1}$$

where κ is the surface wave-number, $\kappa_p = \sqrt{2\beta/3}g/U^2$ is the wave number at which the spectrum has a peak and $\alpha = 8.1 \times 10^{-3}$, $\beta = 0.74$, $g = 9.81 \text{ m/sec}^2$. The RMS surface height deviation, $\sigma_h = \sqrt{\alpha}/\sqrt{6}\kappa_p$ and the RMS correlation length of the surface $\rho_c = 5/2\sqrt{2}\kappa_p$. The PM spectrum for $U = 10 \text{ m/sec}$ would look like Figure 1 below. The corresponding correlation function $C(x; k_p)$ shown in Figure 2 can be obtained by taking the inverse Fourier transform of $W(k)$ or by evaluating the integral^[11] in Eq. 2.1.2:

$$C(x; k_p) = \int_0^\infty \frac{2e^{-1/y^2}}{y^3} \cos(\sqrt{1.5} k_p y x) dy \quad \text{Eq. 2.1.2}$$

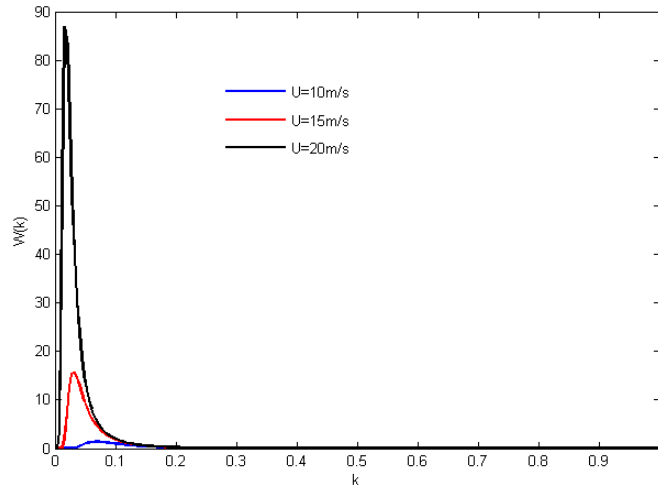


Figure 1: PM Spectrum for varying wind speeds

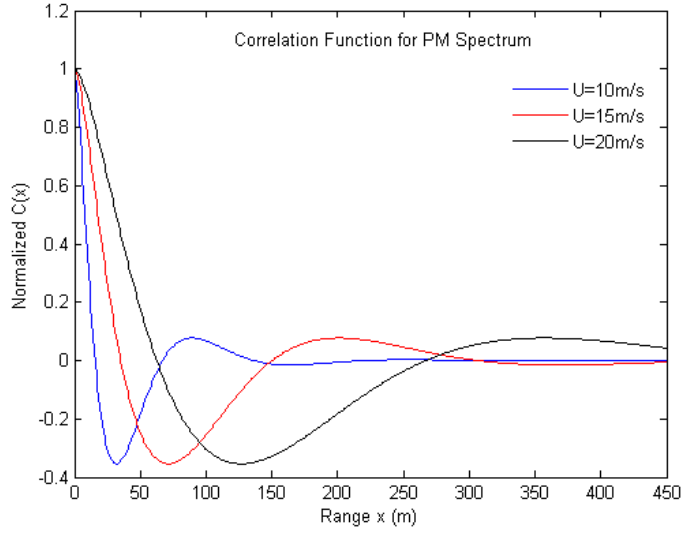


Figure 2: Correlation function for the PM spectrum for varying wind speeds

The correlation function $C(x; k_p)$ depends on the wind-speed through wave-number κ_p . By truncating with an appropriate finite upper limit for y , the integral in Eq. 2.1.2 can be numerically evaluated by taking into account:

$$\lim_{y \rightarrow 0} \frac{e^{-1/y^2}}{y^3} = 0 \quad \text{Eq. 2.1.3}$$

The Gaussian pdf $p(x)$ in this case takes the form below:

$$p(x) = \frac{1}{\sigma_h \sqrt{2\pi}} e^{-\frac{(x-\mu)^2}{2\sigma_h^2}} \quad \text{Eq. 2.1.4}$$

In accordance to the procedure outlined in [13], one can arrive at the random one dimensional surface function $g(x)$ with zero mean ($\mu=0$) and root mean square (RMS) height σ_h by making a change of variables from the time domain t , to the horizontal range domain x , and correspondingly from angular frequency domain ω , to the wave-number domain k . In other words, the spatial domain bears similarity with the time domain and wave-number domain $k/2\pi$, with the frequency domain f .

Let us assume $g(x)$ is the real random process which we would like to obtain for the rough surface that extends from $x=0$ to $x=X_{max}$. If $W(k)$ is its power spectral density, then

$$W(k) = \lim_{X_{max} \rightarrow \infty} \frac{\langle |\tilde{g}(k)|^2 \rangle}{X_{max}} \quad \text{Eq. 2.1.5}$$

where, “ $\langle \ \rangle$ ” symbol represents the ensemble mean and $\tilde{g}(k)$ is the Fourier transform of $g(x)$.

Let us define $h(x)$ such that

$$h(x) = g(x) + \bar{x} \quad \text{Eq. 2.1.6}$$

where, \bar{x} is the mean of the random process defining the rough surface. In our case, the random process is a zero mean process, but we will show the expressions without loss of generality. If $H(k)$ is the power spectral density of $h(x)$, then

$$H(k) = W(k) + \bar{x}^2 \delta(k) \quad \text{Eq. 2.1.7}$$

Hence, for the random process $g(k)$, we set

$$\langle |\tilde{g}(k)|^2 \rangle = X_{max} H(k) \triangleq g^2(k) \quad \text{Eq. 2.1.8}$$

The phase of $\tilde{g}(k)$ can be specified subject to the condition:

$$\text{Angle}(\tilde{g}(-k)) = -\text{Angle}(\tilde{g}(k)), \quad k \geq 0 \quad \text{Eq. 2.1.9}$$

so that a real valued process is generated. If σ_h denotes the RMS surface height, then

$$\sigma_h^2 = \langle (x - \bar{x})^2 \rangle \quad \text{Eq. 2.1.10}$$

be the variance of the random process $h(x)$. Random variables are incorporated in the wave-number domain according to the following set:

$$\tilde{g}(n\Delta k) = \begin{cases} g(n\Delta k) \left(\frac{(x_{1n} - \bar{x}) + j(x_{2n} - \bar{x})}{\sigma_h \sqrt{2}} \right), & 1 \leq n \leq \frac{N}{2} - 1 \\ \tilde{g}^*(n\Delta k), & \frac{-N}{2} + 1 \leq n \leq -1 \\ g(0) \frac{x_0 - \bar{x}}{\sigma_h}, & n = 0 \\ g\left(\frac{N\Delta k}{2}\right) \frac{x_{N/2} - \bar{x}}{\sigma_h}, & n = \frac{N}{2} \end{cases} \quad \text{Eq. 2.1.11}$$

where the symbols $x_0, x_{1n}, x_{2n}, x_{N/2}$ are independent random variables generated from the pdf $p(x)$. The reason for choosing real values at $n = 0$ is to ensure the phase condition is met according to Eq. 2.1.9 for $k = 0$ and real value at $k = N/2$ is to ensure periodicity is satisfied by $\tilde{g}(N\Delta k/2) = \tilde{g}(-N\Delta k/2)$. The actual real random process in the x domain can be obtained by taking the discrete Fourier-inverse of Eq. 2.1.11.

In order to prevent aliasing and to ensure the sampling intervals are reasonably sufficient in either domain, we set the following conditions based on the sampling theorem.

$$\begin{aligned}
\Delta x &\leq \frac{\pi}{\kappa_c} \\
\Delta k &\leq \frac{2\pi}{X_{max}} \\
\Delta x * \Delta k &\leq \frac{2\pi}{N} \\
N &\geq \frac{X_{max} * \kappa_c}{\pi}
\end{aligned}
\tag{Eq. 2.1.12}$$

A single realization of the rough sea surface with PM spectrum and Gaussian height statistics is shown in Figure 3 for a wind speed $U=10$ m/s.

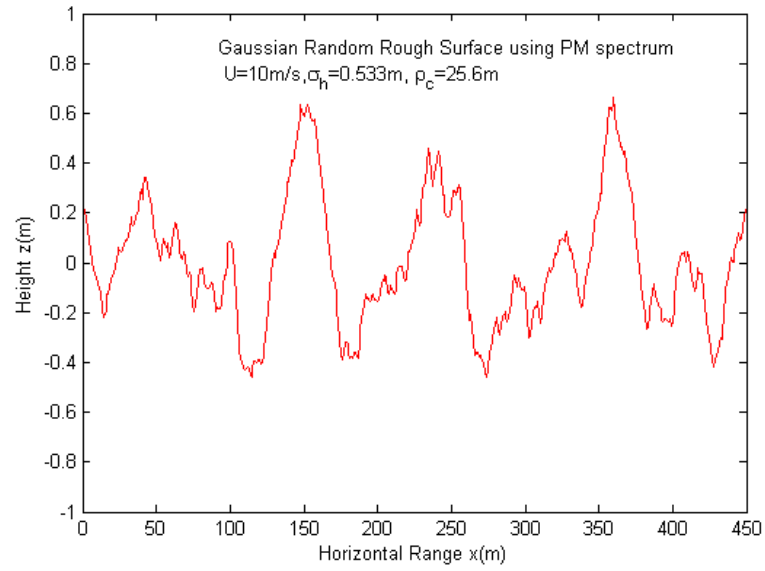


Figure 3: Single realization of random rough sea surface using Gaussian height statistics & PM spectrum, $U=10$ m/s, $\sigma_h=0.533$ m, $\rho_c=25.6$ m, $N_p=512$, $\Delta x=0.88$ m

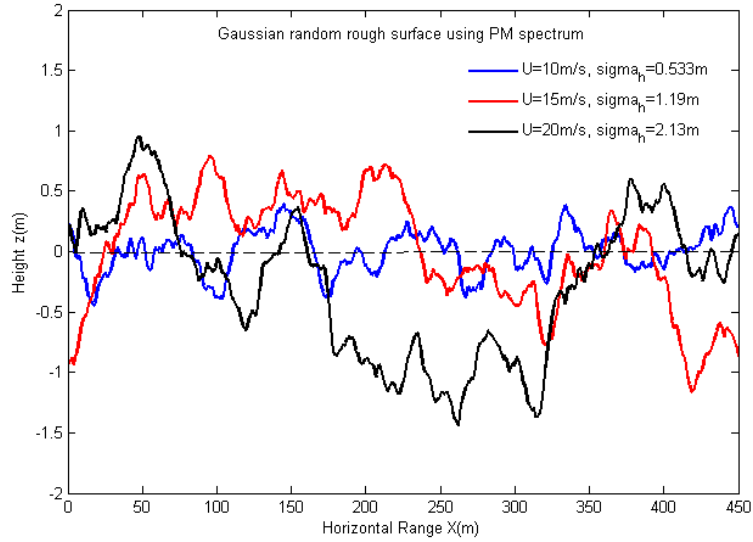


Figure 4: Random rough surfaces at varying wind speeds

In order for the discretized random process to satisfy the sampling rate theorem, the condition that needs to be satisfied is:

$$\Delta x \cdot \Delta \kappa \leq \frac{2\pi}{N} \quad \text{Eq. 2.1.13}$$

where $\Delta x = \frac{X_{max}}{N}$, $\Delta \kappa = \frac{2\kappa_c}{N}$ and $\kappa_c = 51 \kappa_p$. The quantity κ_c is the cut-off wavenumber for the PM spectrum and N is the number of points in the discrete version of the random process. If the spectrum or the maximum horizontal range is too narrow, a step size in one domain may make the step size in other domain too large according to Eq. 2.1.13. This would result in poor resolution in that domain. To avoid this, the spectrum $W(k)$ or the spatial domain signal $g(x)$ can be padded with zeroes to artificially increase κ_c or X_{max} . If one of Δx or $\Delta \kappa$ is fixed by the aliasing requirement, the other can be obtained for a given N . The step sizes are adjusted such that $N = 2^n$ for some integer n . This is also a requirement of standard FFT algorithms for its implementation.

CHAPTER 3

INDUCED CURRENT DENSITY

The chapter describes the essential steps to formulate and compute the induced current density on the surface due to incident waves as a function of the horizontal distance. This is done using the PE equation, the properties of Green's function and applying suitable boundary conditions. The boundary under consideration here consists of the rough surface, the z axis ($x=0$) containing the transmitter antenna, a vertical line parallel to the z axis at some horizontal observation distance from the origin and the infinite space above the surface.

3.1. Direct & Exact Solution

A Volterra Integral Equation of the second kind ^[7] derived using the properties of Green's function that satisfies the Parabolic Equation (PE) is used for the solution to the unknown current density $J(x)$. Since the slopes of the rough surface are small, the back-scattering of the waves is ignored and waves travelling within $\pm 10^\circ$ - 17° ¹ to the horizontal axis can be accurately modeled in this method. A time harmonic dependence of $e^{-i\omega t}$ is considered and suppressed throughout. Hence, the reduced field $U = e^{-ik_0 x} E_y$ satisfies the standard parabolic equation for a wave travelling in the positive x direction. The fields are assumed to be generated by a vertically polarized magnetic source placed in the y - z plane, resulting in a mode with non-zero field components of E_y , H_x and H_z , where E and H denote electric and magnetic field respectively. The rough surface is described by $z=g(x)$ and the medium above it is taken to be vacuum with permittivity ϵ_0 and permeability μ_0 .

¹ Based on comparison of $\cos \psi$ and $1-(\sin^2 \psi)/2$, where ψ is the grazing angle and assuming 0.1% tolerance.

The theory and procedure outlined in [7] is followed using Green's function that satisfies the PE equation and Volterra integral equation of the second kind to obtain the total field above rough surface. Let us denote the total field above the rough surface at any point x, z as $U(x, z)$. $U(x, z) = U_{inc}(x, z) + U_s(x, z)$, where U_{inc} and U_s are the incident and scattered fields respectively. It can be shown that:

$$U(x, z) = \int_{g_0}^{\infty} U_0(\eta) G_0(x, z; 0, \eta) d\eta - \frac{i}{2k_0} \int_0^x J(\xi) G_0(x, z; \xi, g(\xi)) d\xi \quad \text{Eq. 3.1.1}$$

hence,

$$U_{inc}(x, z) = \int_{g_0}^{\infty} U_0(\eta) G_0(x, z; 0, \eta) d\eta \quad \text{Eq. 3.1.2}$$

$$U_s(x, z) = -\frac{i}{2k_0} \int_0^x J(\xi) G_0(x, z; \xi, g(\xi)) d\xi \quad \text{Eq. 3.1.3}$$

where $G_0(x, z; \xi, g(\xi))$ is the Green's function evaluated at $x=\xi$ and $z=g(\xi)$ and satisfies the PE equation. It is given by:

$$G_0(x, z; \xi, \eta) = \frac{\gamma \Theta(x - \xi)}{\sqrt{(x - \xi)}} \exp \left[\frac{ik_0}{2} \frac{(z - \eta)^2}{(x - \xi)} \right] \quad \text{Eq. 3.1.4}$$

where $\gamma = \sqrt{\frac{k_0}{2\pi i}}$ and $\Theta(x)$ is the unit step function. In its integral form, the Green's function can also be expressed as:

$$G_0(x, z; \xi, \eta) = \frac{\Theta(x - \xi)}{2\pi} \int_{-\infty}^{\infty} e^{ik_z(z-\eta)} e^{-\frac{ik_z^2}{2k_0}(x-\xi)} dk_z \quad \text{Eq. 3.1.5}$$

The quantity $U_0(\eta)$ is the initial field at $x = 0$ produced by the transmitter antenna of height H_t which is assumed as having a source field Gaussian distributed with amplitude A and standard deviation σ_z . The quantity $g_0=g(x)$ when $x=0$, η is a variable along the z coordinate and ξ along the x coordinate. Free space wave-number is denoted as $k_0 = 2\pi/\lambda$. The initial field then takes the form:

$$U_0(\eta) = \frac{A}{\sqrt{2\pi}\sigma_z} e^{-\frac{(\eta-H_t)^2}{2\sigma_z^2}} \quad \text{Eq. 3.1.6}$$

Based on properties of the free-space Green's function, the following can be derived:

$$\lim_{z \rightarrow g(x)} \frac{1}{ik_0} \frac{\partial G_0}{\partial z} [x, z; \xi, g(\xi)] = \delta(x - \xi) + g_d(x; \xi) G_0[x, g(x); \xi, g(\xi)] \quad \text{Eq. 3.1.7}$$

The following Volterra integral equation of the second kind providing exact solution to current density can then be obtained by using Eq. 3.1.7 in Eq. 3.1.1.

$$J(x) = J_i(x) + \gamma \int_0^x \frac{K_0(x; \xi)}{\sqrt{x - \xi}} J(\xi) d\xi \quad \text{Eq. 3.1.8}$$

where $J_i(x)$ is the incident current density dependent only on the initial conditions at $x=0$ and source field distribution $U_0(\eta)$. $K_0(x; \xi)$ is the kernel of the integral and is defined as:

$$K_0(x; \xi) = g_d(x; \xi) \exp[ik_0(x - \xi)g_d^2(x; \xi)/2] \quad \text{Eq. 3.1.9}$$

where $g_d(x; \xi)$ is given as:

$$g_d(x; \xi) = \frac{g(x) - g(\xi)}{x - \xi} \quad \text{Eq. 3.1.10}$$

$K_0(x; x) = g'(x)$, which is the first order derivative function of the rough surface.

An integral equation for $J(x)$ may be formulated using $(x) = \frac{\partial U_s}{\partial \eta}$, by differentiating Eq. 3.1.1 with respect to z and applying the limit^[14] $\lim_{z \rightarrow g(x)}$ [14]. Using properties of Green's function, the incident current density is then given as

$$J_i(x) = -2 \int_{g_0}^{\infty} U_0(\eta) \frac{\partial}{\partial \eta} G_0[x, g(x); 0, \eta] d\eta \quad \text{Eq. 3.1.11}$$

and depends only on the initial source field distribution and surface profile function $g(x)$. Using the source field specified in Eq. 3.1.6 and the integral in Eq. 3.1.11, we obtain the incident current density as

$$J_i(x) = \frac{A(H_t - g(x))}{(\sigma_z^2 + ix/k_0)^{3/2}} \sqrt{\frac{2}{\pi}} \exp \left[-\frac{(H_t - g(x))^2}{2(\sigma_z^2 + ix/k_0)} \right] \quad \text{Eq. 3.1.12}$$

Eq. 3.1.12 is valid for $(H_t - g_0) \gg \sigma_z$.

3.2.Zeroth Order Solution

As we can see from Eq. 3.1.8, the unknown quantity $J(\xi)$ is part of the integrand, which makes it an integral equation whose numerical solution would be computationally intensive. Since the Volterra integral equation of the second kind as in Eq. 3.1.8 solves for the current at a given point in terms of the current at all previous points, a marching procedure needs to be adopted due to its causal nature. This becomes laborious especially at very large horizontal ranges. Hence, we use zeroth order current density solution $J^{(0)}(x)$ which is a good approximation of the exact numerical current density and involves computing an integral wherein the integrand is now a function of the known incident current density $J_i(x)$ and can be obtained from Eq. 3.1.12. The zeroth order current density is given by:

$$J^{(0)}(x) = J_i(x) + \gamma \int_{x'=0}^x J_i(x') \frac{K_0(x; x')}{\sqrt{(x - x')}} dx' \quad \text{Eq. 3.2.1}$$

In order to remove the weak singularity that exists in Eq. 3.2.1 at $x' = x$, an alternate form of the equation with change of variables is used.

$$J^{(0)}(x) = J_i(x) + 2\gamma\sqrt{x} \int_{\theta=0}^{\pi/2} J_i(x \sin^2\theta) K_0(x; x \sin^2\theta) \sin\theta d\theta \quad \text{Eq. 3.2.2}$$

A comparison of the absolute values of exact numerical current density (J^{num}) with the zeroth order solution (J^0) is shown in Figure 5 for a single realization of a random rough surface. Figure 6 compares the phase of J^{num} and J^0 and it can be observed that zeroth order solution matches reasonably well with the exact solution barring a few peaks and troughs.

The exact solution to Eq. 3.1.8 can be expressed in the form of an infinite series expansion using the theorem pertaining to Volterra integral equation of the second kind as shown below:

$$J(x) = J^{(0)}(x) + \sum_{n=1}^{\infty} \gamma^{2n} \int_0^x K_n(x; t) J^{(0)}(t) dt \quad \text{Eq. 3.2.3}$$

where the kernels $K_n(x; t)$ satisfy the recurrence relation

$$K_n(x; t) = \int_{\xi=t}^x K_1(x; \xi) K_{n-1}(\xi; t) d\xi \text{ for } n \geq 2 \quad \text{Eq. 3.2.4}$$

It is to be noted that for any $t > x$, the kernels $K_n(x; t) = 0$ for $n=1, 2$, so forth. Computation of the exact solution from the infinite series expansion involves computing the zeroth order current density from Eq. 3.2.2, solving for the kernels from Eq. 3.2.4 and then using these in Eq. 3.2.3. The amount of computational labor depends on the number of terms used in the series, the nature of the rough surface, the maximum range, and the integration scheme employed.

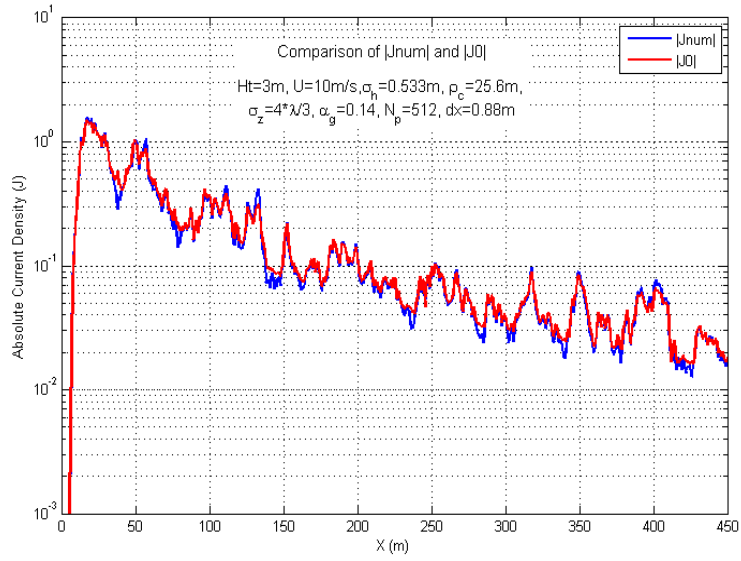


Figure 5: Comparison of absolute J^{num} and J^0 for a wind-generated PM random rough surface at 1 GHz, $\lambda = 0.3\text{m}$, $H_t = 3\text{m}$, $U = 10\text{m/s}$, $\sigma_n = 0.533\text{m}$, $\rho_c = 25.6\text{m}$, $N_p = 512$, $\Delta x = 0.88\text{m}$, $\sigma_z = 4\lambda/3$, max. absolute slope $\alpha_g = 0.14$

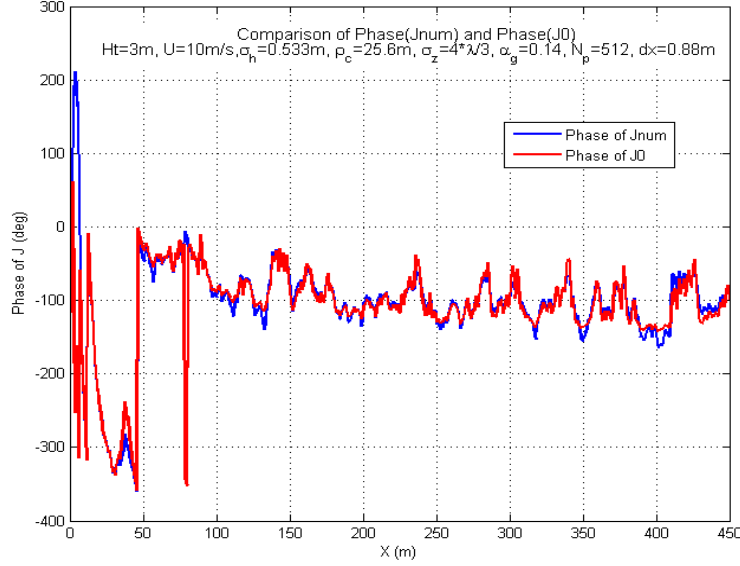


Figure 6: Phase (degrees) of J^{num} and J^0 for a wind-generated PM random rough surface at 1 GHz, $\lambda=0.3\text{m}$, $H_t=3\text{m}$, $U=10\text{m/s}$, $\sigma_h=0.533\text{m}$, $\rho_c=25.6\text{m}$, $N_p=512$, $\Delta x=0.88\text{m}$, $\sigma_z=4\lambda/3$, max. absolute slope $\alpha_g=0.14$

The surface properties for which the current densities are computed are as follows: wind speed ($U=10\text{m/s}$), RMS height of surface ($\sigma_h=0.53\text{m}$), correlation length of surface ($\rho_c=25.6\text{m}$), maximum absolute slope of the surface ($\alpha_g=0.14$), number of points N considered for the sampling of surface ($N=512$), maximum horizontal range ($X=450\text{m}$) and distance between adjacent samples on the surface is $\Delta x=0.87\text{m}$. The frequency of the incident wave is $f=1\text{ GHz}$ and antenna height $H_t=3\text{m}$. The RMS surface height per unit wavelength $\sigma_h/\lambda = 1.77$ and surface correlation length $\rho_c/\lambda = 85.33$. Since for the PM spectrum the ratio of σ_h/ρ_c is a constant, we consider the parameter σ_h/λ for our further analysis. We observe that the zeroth order solution agrees well with the exact numerical solution in this case. Implementing the routine in Matlab with a system having 3.2 GHz, 3rd generation Intel quad-core processor, it is determined that while the computation time for J^{num} is 24.06 sec, J^0 takes 0.46 sec which is about 50 times faster, without significantly compromising on the accuracy of the solution.

CHAPTER 4

PROPAGATION FACTOR

Once the induced current densities are determined from the steps outlined in Chapter 3, we then analyze the computation of scattered field that arise due to these currents. The propagation factor is the ratio of the total field above the surface to the incident field. This factor is a more intuitive parameter that helps us understand the pattern of wave propagation in free space over a rough surface. The propagation factor accounts for the effects of multipath and shadowing, subject to the forward propagation approximation. In real-world situations, path loss effects should also be considered ^[15].

4.1.Scattered field along a vertical line

Using the exact numerical solution to induced current density (Eq. 3.1.8) and zeroth order current density (Eq. 3.2.2), the corresponding scattered field at along a vertical line (z) at the maximum horizontal range ($X=450\text{m}$) is computed using Eq. 3.1.3. We adopt the approach outlined by Lai ^{[8][8]}, wherein the surface function $g(x)$ and current density $J(x)$ are both linearly approximated in a given sample interval (x_n, x_{n+1}) as follows

$$g(x) = g_n + \frac{(x - x_n)(g_{n+1} - g_n)}{\Delta x} \quad \text{Eq. 4.1.1}$$

$$J(x) = J_n + \frac{(x - x_n)(J_{n+1} - J_n)}{\Delta x} \quad \text{Eq. 4.1.2}$$

where $g_n = g(x_n)$, the surface function value at a point x_n for $1 \leq n \leq N - 1$, N being the total number of sample points on the surface, and $\Delta x = x_{n+1} - x_n$. Similarly we assign $J_n = J(x_n)$. We use a discretized version of Eq. 3.1.8 corresponding to the scattered field $U_s(x, z)$ which can be expressed as a sub-integral as follows:

$$I_n = - \sqrt{\frac{i}{8\pi k_0}} \int_{x_n}^{x_{n+1}} \frac{J(x')}{\sqrt{(x - x')}} \exp \left\{ i \frac{k_0}{2} \frac{|z - g(x')|^2}{x - x'} \right\} dx' \quad \text{Eq. 4.1.3}$$

Using the linear discretized version of $J(x)$, $g(x)$ and making appropriate change of variables, the sub-integral then becomes:

$$I_n = -\frac{e^{iD_n}}{\pi} \sqrt{\frac{i|C_n|}{2k_0}} \int_{t_{1n}}^{t_{2n}} \left(\frac{A_n}{t^2} - \frac{B_n}{t^4} \right) e^{\pm \frac{i\pi t^2}{2}} dt \quad \text{Eq. 4.1.4}$$

This can be integrated by parts and expressed in terms of Fresnel integrals. These sub-integrals are summed over $1 \leq n \leq N - 1$ to solve for the scattered field ($U_s(x, z)$) at a given point (x, z) above the rough surface.

$$I_n = -\frac{e^{iD_n}}{\pi} \sqrt{\frac{i|C_n|}{2k_0}} \left\{ \pi \left(\pm iA_n + \frac{\pi B_n}{3} \right) [F_{\pm}(t_{2n}) - F_{\pm}(t_{1n})] \right. \\ \left. + \frac{1}{t_{2n}} \left(-A_n \pm \frac{i\pi B_n}{3} + \frac{B_n}{3t_{2n}^2} \right) e^{\pm i\pi t_{2n}^2/2} \right. \\ \left. - \frac{1}{t_{1n}} \left(-A_n \pm \frac{i\pi B_n}{3} + \frac{B_n}{3t_{1n}^2} \right) e^{\pm i\pi t_{1n}^2/2} \right\} \quad \text{Eq. 4.1.5}$$

Where

$$C_n = k_0(z - g_n)[(z - g_n) - 2(x - x_n)(g_{n+1} - g_n)/\Delta x] \quad \text{Eq. 4.1.6}$$

$$D_n = k_0(z - g_n)[(g_{n+1} - g_n)/\Delta x] \quad \text{Eq. 4.1.7}$$

$$t_{1n} = \sqrt{|C_n|/[\pi(x - x_n)]} \quad \text{Eq. 4.1.8}$$

$$t_{2n} = \sqrt{|C_n|/[\pi(x - x_{n+1})]} \quad \text{Eq. 4.1.9}$$

$$A_n = J_n + (N - n + 1)(J_{n+1} - J_n) \quad \text{Eq. 4.1.10}$$

$$B_n = |C_n|(J_{n+1} - J_n)/(\pi\Delta x) \quad \text{Eq. 4.1.11}$$

F_+ and F_- are the Fresnel integral and its complex conjugate respectively. I_n takes the '+' sign for $C_n \geq 0$ and '-' sign for $C_n < 0$ respectively.

Let us denote the scattered field computed using J^{num} as U_s^{num} and using J^0 as U_s^0 respectively. The incident field at any point (x, z) is denoted by $U_i(x, z)$, can be computed using the Fourier transform of the initial field $U_o(\eta)$. If $U_o(k_z)$ is the Fourier transform of $U_o(\eta)$, then the incident field corresponding to Eq. 3.1.2 is given by^[14]:

$$U_{inc}(x, z) = \frac{1}{2\pi} \int_{-\infty}^{\infty} U_o(k_z) e^{\frac{-ik_z^2 x}{2k_0}} e^{ik_z(z-g_0)} dk_z \quad \text{Eq. 4.1.12}$$

and takes the form

$$U_{inc}(x, z) = \frac{A\sigma_z}{\sqrt{\sigma_z^2 + ix/k_0}} \exp \left[-\frac{(z - H_t)^2}{2(\sigma_z^2 + ix/k_0)} \right] \quad \text{Eq. 4.1.13}$$

Although the limits of k_z in the integral of Eq. 4.1.12 extend to infinity, in reality the angular limitation of PE equation truncates the limits to the order of $k_0 \sin(\theta_{max})$, where θ_{max} is approximately 15° grazing angle. The propagation factor (PF) is defined as the ratio of the total field to the incident field. $PF (dB) = 20 \log_{10}(|\frac{U_s + U_{inc}}{U_{inc}}|)$ For $x=X_{max}=450m$, the propagation factor is plotted as a function of z for a single realization of a random surface with the same characteristics used in Figure 5.

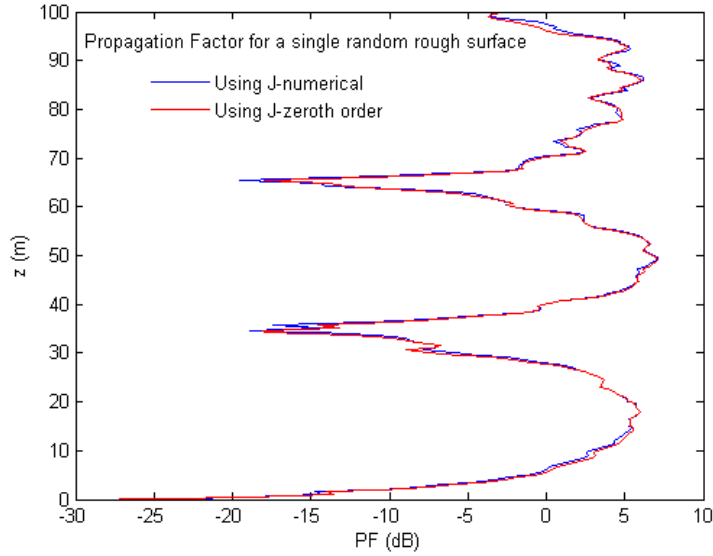


Figure 7: PF for a single realization of a PM surface

The mean propagation factor is obtained by determining the current densities (both J_{num} and J_0) for a single realization of a surface, computing the scattered field (for each of J_{num} and J_0) for that realization, repeating the process for $N_r=400$ realizations of the rough surface and taking the mean scattered field of these “ N_r ” U_s values. The value of N_r is taken as 400 after analyzing the mean field for various incremental values of N_r starting from 100 in accordance to the Monte-Carlo method and concluding that the mean propagation factor converged to a reasonable statistical moment for $N_r=400$.

The mean propagation factor (PF) based on the mean field is equal to $20 \log_{10}(|\frac{\langle U_s \rangle + U_{inc}}{U_{inc}}|)$, where $\langle U_s \rangle$ is the ensemble average of the complex scattered field of all surface realizations.

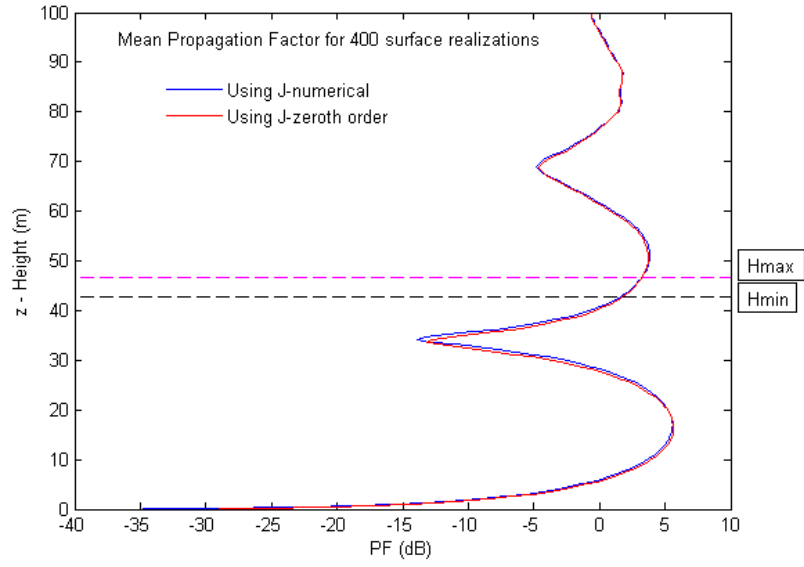


Figure 8: Mean PF for 400 realizations of PM surface

We observe the agreement between the propagation factors generated using J^{num} and J^0 is better in the mean field computation rather than the single surface realization as expected. The mean scattered field is small compared to the incident field at large heights due to smaller diffused non-specular components and hence the PF converges to the incident field. Specular reflection occurs up to a height when the angle of incidence is equal to the angle of reflection from the mean surface for a wave incident from the lower half beam of the transmitting antenna. This height is denoted as H_{min} . The height up to which we have direct incidence from the upper half beam of the transmitting antenna (see Figure 9) is denoted as H_{max} .

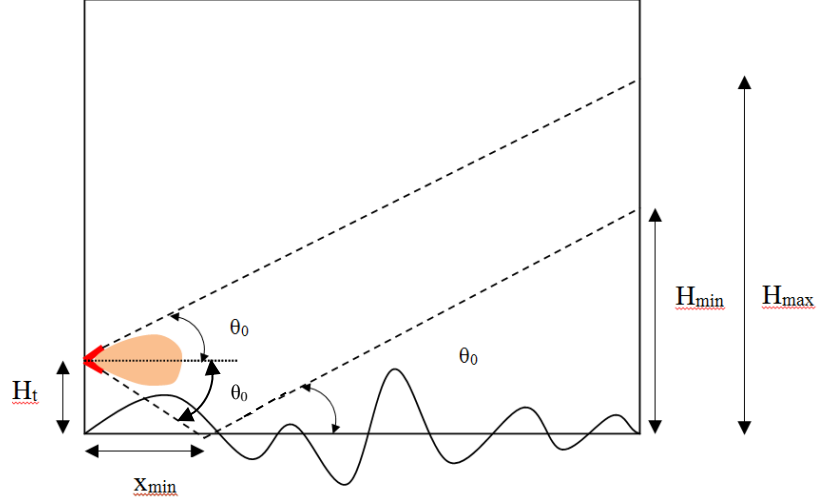


Figure 9: Schematic depicting the specular reflection and direct incidence

From laws of reflection, we can arrive at the equations for H_{min} and H_{max} taking maximum horizontal range $X=450\text{m}$.

$$H_{min} = X \tan \theta_0 - H_t \quad \text{Eq. 4.1.14}$$

$$H_{max} = X \tan \theta_0 + H_t \quad \text{Eq. 4.1.15}$$

The half beam angle of the transmitting antenna is determined by the standard deviation σ_z of the Gaussian distribution of its source field ^[13]. The half-power beam-width of the transmitting antenna is denoted as $\Delta\psi=2\theta_0$.

$$\Delta\psi = 2 \tan^{-1} \left(\frac{\tan \psi_1}{\sqrt{1.443}} \right) \quad \text{Eq. 4.1.16}$$

where

$$\psi_1 = \tan^{-1} \left(\frac{1}{\sigma_z k_0} \right) \quad \text{Eq. 4.1.17}$$

Thus for $\sigma_z = 4\lambda/3$ and $\lambda=0.3\text{m}$, the half power beam width of the antenna, $\Delta\psi=11.34^\circ$ and $\theta_0=5.67^\circ$. For an antenna height $H_t=2\text{m}$ and $X=450\text{m}$, $H_{min}=42.67\text{m}$ and $H_{max}=46.67\text{m}$. Thus beyond 46.67m, the field is only composed of the non-specular reflections.

4.2. Zeroth Order Asymptotic Expression

Since the zeroth order results are in good agreement with the exact solution, we use an asymptotic form of the specular mean scattered field derived using zeroth order induced current density J^0 [11]. The scattered field given by Eq. 3.1.3 is considered. The induced current density $J(\xi)$ is replaced with zeroth order current density J^0 . Using the statistical properties of the Gaussian surface and Beckmann's mean value theorem [16] in Eq. 4.2.1 for random variables as exponents, the mean scattered field is determined. This asymptotic mean scattered field is denoted as $\langle U_s^0 \rangle = \langle U_{s1}^0 \rangle + \langle \Delta U_s^0 \rangle$.

$\langle U_{s1}^0 \rangle$ is the mean scattered field due to incident current density J_i , the first term of zeroth order induced current density in Eq. 3.2.1. This term corresponds to the specular reflections from the surface and yields the Ament roughness reduction factor in Eq. 4.2.15. The $\langle \Delta U_s^0 \rangle$ term takes into account the correlation function of the surface through the second term of Eq. 3.2.1.

$$\langle g(x) * g(x') \rangle = \sigma_h^2 C(|x - x'|) \quad \text{Eq. 4.2.1}$$

where C is the correlation function of the surface as specified in Eq. 2.1.2.

$$\langle U_{s1}^0 \rangle = -\sqrt{\frac{k_0}{2\pi i x}} \Psi_0(-k_0 \tan \theta_2) \exp[-2(k_0 \sigma_h \tan \theta_2)^2] \exp[ik_0(z + H_t) \tan \theta_2 / 2] \quad \text{Eq. 4.2.2}$$

where,

$$\Psi_0(k_z) = U_0(k_z) e^{-ik_z H_t} \quad \text{Eq. 4.2.3}$$

$U_0(k_z)$ is the Fourier transform of the source field distribution in Eq. 3.1.6.

$$\tan \theta_2 = \frac{(z + H_t)}{x} \quad \text{Eq. 4.2.4}$$

An asymptotic form of the incident field $U_i(x, z)$ in Eq. 4.1.13 can also be written as

$$U_i = \sqrt{\frac{k_0}{2\pi ix}} \Psi_0(k_0 \tan \theta_1) \exp[ik_0(z - H_t) \tan \theta_1 / 2] \quad \text{Eq. 4.2.5}$$

$$\text{where} \quad \tan \theta_1 = \frac{(z - H_t)}{x} \quad \text{Eq. 4.2.6}$$

The expression in Eq. 4.2.2 only takes into account the specular reflection. In order to present the complete scenario, the diffused components corresponding to the zeroth order approximation should also be added to give the total mean scattered field. Using the Beckmann's mean value theorem^[16] and statistical properties of Gaussian surface as well as the correlation function corresponding to the PM spectrum, the mean diffused scattered field $\langle \Delta U_s^0 \rangle$ can be found as:

$$\begin{aligned} \langle \Delta U_s^0 \rangle = & \frac{\sqrt{\pi} k_0 (k_0 \sigma_h)^2}{(2\pi)^3} \iiint_{-\infty}^{\infty} (v \\ & + u) \Psi_0 \left(\frac{k_0(v + u)}{2} \right) e^{\frac{i[k_0 v(z - H_t) - k_0 u(z + H_t)]}{2}} * \\ & \frac{(1 - C(x))}{[(k_0 \sigma_h)^2 (1 - C(x)) + ip_1]^{\frac{3}{2}}} \frac{\sin\left[\frac{uv(P - p_1)}{2}\right]}{u} e^{-\sigma_u^2 u^2} e^{-\sigma_v^2 v^2} du dv dp_1 \end{aligned} \quad \text{Eq. 4.2.7}$$

In order to make the three dimensional integral limits finite in all the domains and for ease of numerical computation, we convert the integration space to cylindrical coordinates by making a change of variables as $u = \rho \sin(\alpha)$ and $v = \rho \cos(\alpha)$ and rewrite the equation as:

$$\begin{aligned} & \langle \Delta U_s^0 \rangle \\ & = \frac{\sqrt{\pi} k_0 (k_0 \sigma_h)^2}{(2\pi)^3} \iiint_{0}^{\rho_{2\pi p}} \rho(\sin(\alpha)) \\ & + \cos(\alpha)) \Psi_0 \left(\frac{k_0 \rho(\sin(\alpha) + \cos(\alpha))}{2} \right) e^{\frac{ik_0 \rho [\cos(\alpha)(z - H_t) - \sin(\alpha)(z + H_t)]}{2}} * \end{aligned} \quad \text{Eq. 4.2.8}$$

$$\frac{(1 - C(x)) \sin \left[\frac{\rho^2 \sin(2\alpha) (P - p_1)}{4} \right]}{[(k_0 \sigma_h)^2 (1 - C(x)) + ip_1]^{\frac{3}{2}} \sin(\alpha)} * \\ e^{-\sigma_u^2 \rho^2 \sin^2(\alpha)} e^{-\sigma_v^2 \rho^2 \cos^2(\alpha)} d\rho d\alpha dp_1$$

The function Ψ_0 bears the same definition as in Eq. 4.2.3. $C(x)$ is the normalized correlation function corresponding to the PM spectrum as defined in Eq. 2.1.2. The quantity $P = k_0 * \frac{x_{max}}{2}$ is a constant for a given maximum range and $p_1 = k_0 * \frac{x}{2}$

The quantities σ_u^2 and σ_v^2 are defined as follows:

$$\sigma_u^2 = \frac{(k_0 \sigma_h)^2}{4} (1 + C(x)) + \frac{i}{4} (P - p_1) \quad \text{Eq. 4.2.9}$$

$$\sigma_v^2 = \frac{a_1 p_1^2}{4(a_1^2 + p_1^2)} + \frac{i}{4} \left(P - \frac{p_1^3}{a_1^2 + p_1^2} \right) \quad \text{Eq. 4.2.10}$$

where $a_1 = [1 - C(x)](k_0 \sigma_h)^2$ and is always greater than or equal to zero.

Hence, the total mean scattered field corresponding to the asymptotic zeroth order expression is:

$$\langle U_s^0 \rangle = \langle U_{s1}^0 \rangle + \langle \Delta U_s^0 \rangle \quad \text{Eq. 4.2.11}$$

The propagation factor with these asymptotic field expressions would then be $PF (dB) =$

$$20 \log_{10} \left\{ \left| \frac{\langle U_s^0 \rangle + U_i}{U_i} \right| \right\}$$

A comparison between the mean propagation factors computed using J^{num} , J^0 , zeroth order asymptotic expressions, Miller-Brown ^{[9][15]} and Ament ^[10] is shown in Figure 10.

In case of Miller-Brown and Ament formulae, we use the image of the source field representation $U_{inc-image}(x, z)$ i.e. incident field due to image of the source antenna about the mean surface ($x=0$ in this case) to compute the reflected field U_{ref} using the corresponding roughness reduction factor (RRF).

$$U_{inc-image}(x, z) = \frac{A\sigma_z}{\sqrt{\sigma_z^2 + ix/k_0}} \exp \left[-\frac{(z + H_t)^2}{2(\sigma_z^2 + ix/k_0)} \right] \quad \text{Eq. 4.2.12}$$

Note the change in sign to $+H_t$ from $-H_t$ from the expression in Eq. 4.1.13 to denote the image of the source. The reflection co-efficient Γ is equal to -1 . Hence, the mean reflected field $\langle U_{ref} \rangle$ is given as:

$$U_{ref}(x, z) = \Gamma * RRF * U_{inc-image}(x, z) \quad \text{Eq. 4.2.13}$$

The RRF in case of Miller-Brown is given as ^[9]:

$$RRF_{M-B} = e^{-2k_0^2 \sigma_h^2 \sin^2(\varphi)} I_0(2k_0^2 \sigma_h^2 \sin^2(\varphi)) \quad \text{Eq. 4.2.14}$$

where, φ is the grazing angle and I_0 is the zeroth order modified Bessel function of the first kind.

The RRF in case of Ament is given as ^[10]:

$$RRF_{Ament} = e^{-2k_0^2 \sigma_h^2 \sin^2(\varphi)} \quad \text{Eq. 4.2.15}$$

which is the same as Miller-Brown without the Bessel function.

Hence, the total field above the surface is $U_{total}(x, z) = U_{ref}(x, z) + U_{inc}(x, z)$ and the propagation factor (dB) is equal to $20 \log_{10} \left\{ \left| \frac{U_{total}}{U_i} \right| \right\}$.

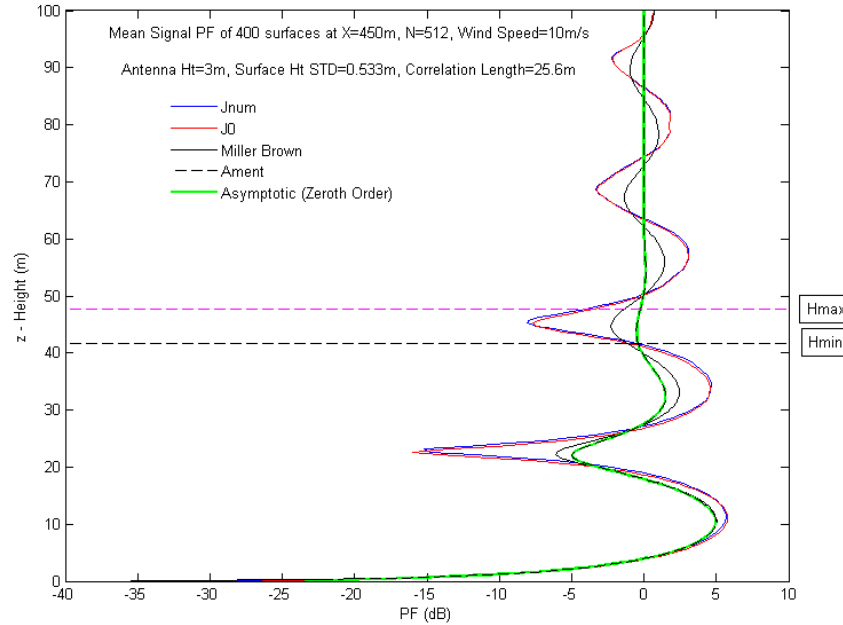


Figure 10: Comparison of Mean PF for 400 surface realizations, $\lambda = 0.3\text{m}$, $H_t = 3\text{m}$, $U = 10\text{m/s}$, $\sigma_h = 0.53\text{m}$, $\rho_c = 25.6\text{m}$, $N_p = 512$, $\Delta x = 0.88\text{m}$, $\sigma_z = 4\lambda/3$, max. absolute slope $\alpha_g = 0.14$

The PF computed from the direct solution to the numerical induced current density and the zeroth order solution agree well with each other for the entire range of height represented above. Miller-Brown, Asymptotic zeroth order and Ament all seem to agree well at low heights up to about 20m, while the asymptotic zeroth order solution matched exactly with the Ament formula. It has been mentioned in prior literature that Miller Brown expression models the propagation more accurately than Ament, but only serves as a reference in this context.

The Miller-Brown and Ament solutions show good match with the numerical and zeroth order solutions at low heights, but flatten relative to the exact numerical solution at large heights implying almost zero contribution to the propagation factor from scattered field. This could be attributed to the fact that both Miller-Brown and Ament solutions are valid in regions where well-defined specular reflected waves exist and multiple scattering from shadowed portions of the surface are ignored. As can be seen from Figure 10, the specular reflection occurs up to a height $H_{min}=41.67\text{m}$ and direct incidence at a height $H_{max}=47.67\text{m}$. Beyond H_{min} , we see that Miller-Brown and Ament are no longer accurate and predominantly constitute of incident field only.

CHAPTER 5

ZEROTH ORDER SOLUTION IN HIGHER FREQUENCY BANDS AND WIND SPEEDS

We now know that the zeroth order current density solution works almost as accurately as the exact solution at 1 GHz and low RMS height of the surface i.e. at wind-speed of 10m/s. It would be interesting to know how well the zeroth order solution agrees with the exact solution at higher wind speeds and surface roughness. We can then define the bounds of validity of the zeroth order solution based on the resulting data analysis.

Further analysis is performed to identify the validity of zeroth order solution at higher frequency of incident radio-waves and wind-speeds (i.e. increased roughness of the surface) for the PM spectrum. The maximum horizontal range is taken as 450 m and maximum vertical height 100 m. One representative mid-band frequency in each of ‘L’, ‘S’, ‘C’ and ‘X’ bands is considered and wind-speeds of 5m/s, 10m/s, 15 m/s and 20 m/s at each of these frequencies is analyzed.

5.1. Mean Signal PF using Monte-Carlo simulations

As before, the scattered field along a vertical line at maximum horizontal range is computed for each realization of the random surface and an ensemble average is taken to yield the mean signal PF = $20 \log_{10}(|\frac{\langle U_s \rangle + U_{inc}}{U_{inc}}|)$. In order to quantify the mismatch between the mean PF due to J_{num} and J_0 , a mean phase error is computed and normalized to the maximum vertical height. Let us denote this quantity as φ_{mean} and is expressed as:

$$\varphi_{mean} = \frac{1}{H_{max}} \int_{z=0}^{H_{max}} |\varphi^{num}(z) - \varphi^0(z)| dz \quad \text{Eq. 5.1.1}$$

where φ^{num} and φ^0 are the unwrapped phase in degrees of the quantities $\frac{\langle U_s^{num} \rangle + U_{inc}}{U_{inc}}$ and $\frac{\langle U_s^0 \rangle + U_{inc}}{U_{inc}}$ respectively. It is observed that the phase mismatch between the exact numerical solution and zeroth order is prominent only in the nulls appearing in the mean

PF and diminish when the PF converges to the incident field. Thus, a more useful parameter would be to normalize the mean phase error φ_{mean} with the number of nulls that are less than 3 dB down from the incident field. The results have been presented and summarized below.

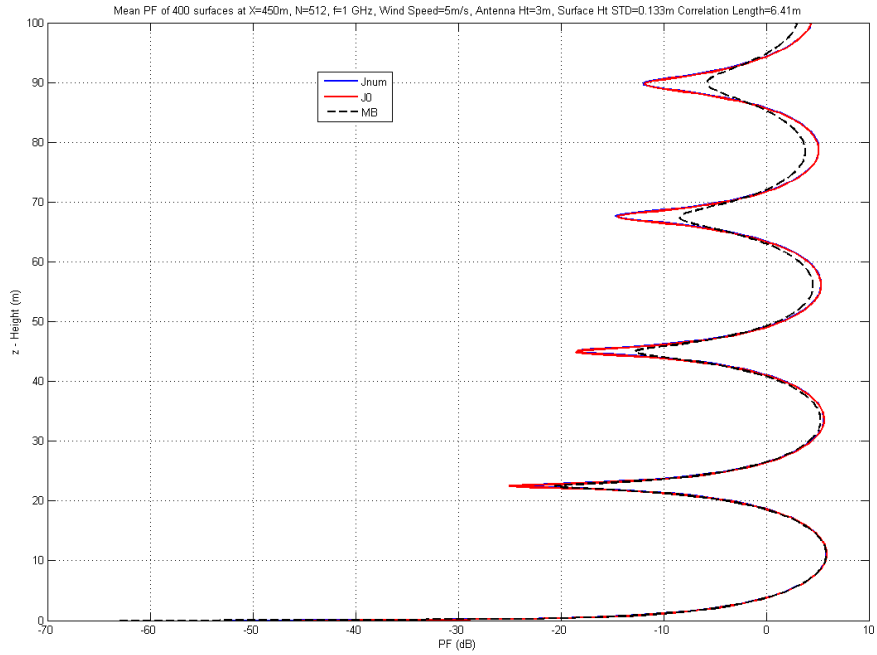


Figure 11: Monte-Carlo mean signal PF of 400 surface realizations at 1 GHz, $\lambda=0.3m$, $H_t=3m$, $U=5m/s$, $\sigma_h=0.13m$, $\rho_c=6.41m$, $N_p=512$, $\Delta x=0.88m$, $X_{max}=450m$

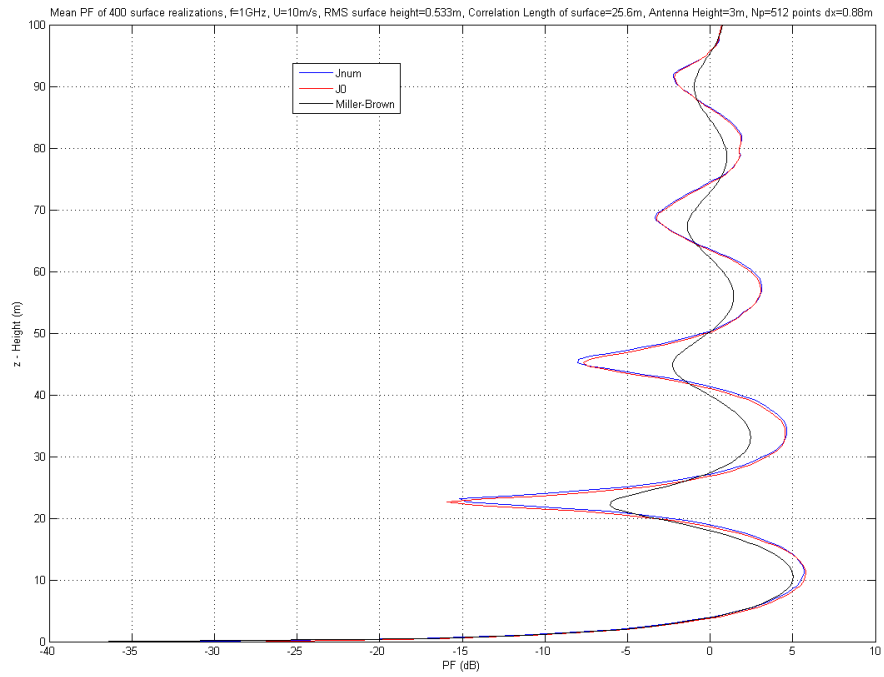


Figure 12: Monte-Carlo mean signal PF of 400 surface realizations at 1 GHz, $\lambda=0.3\text{m}$, $H_t=3\text{m}$, $U=10\text{m/s}$, $\sigma_h=0.53\text{m}$, $\rho_c=25.6\text{m}$, $N_p=512$, $\Delta x=0.88\text{m}$, $X_{max}=450\text{m}$

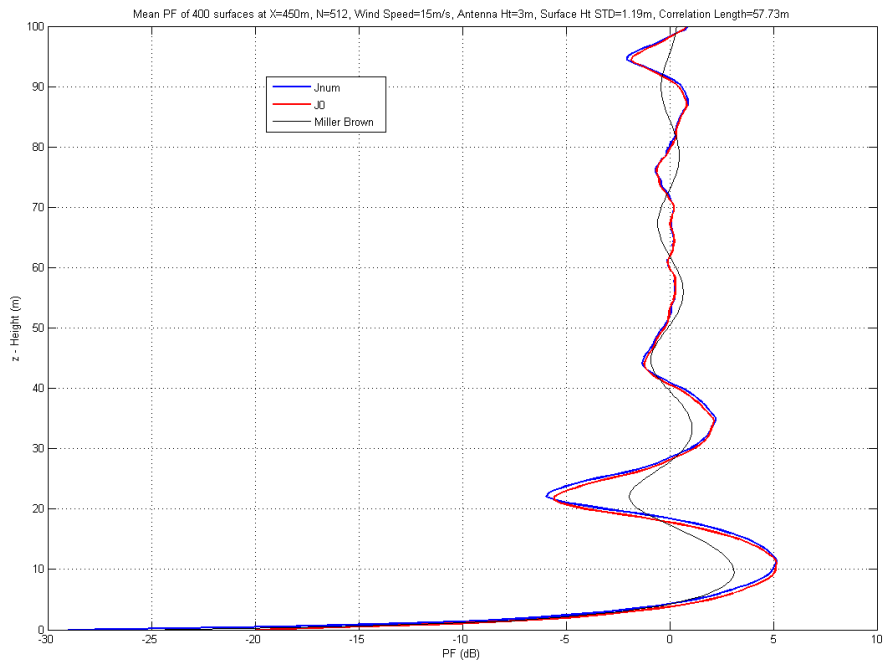


Figure 13: Monte-Carlo mean signal PF of 400 surface realizations at 1 GHz, $\lambda=0.3\text{m}$, $H_t=3\text{m}$, $U=15\text{m/s}$, $\sigma_h=1.19\text{m}$, $\rho_c=57.73\text{m}$, $N_p=512$, $\Delta x=0.88\text{m}$, $X_{max}=450\text{m}$

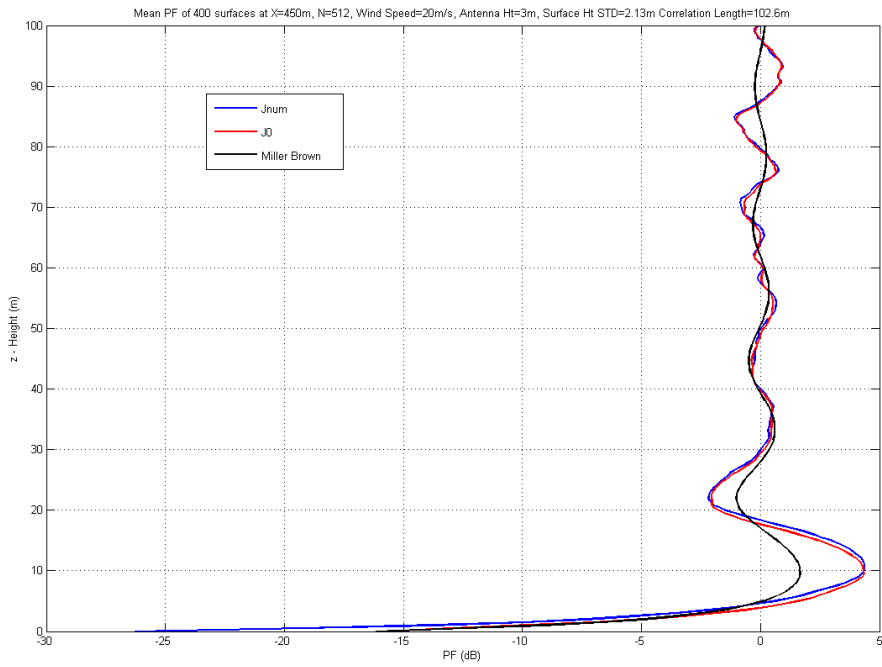


Figure 14: Monte-Carlo mean signal PF of 400 surface realizations at 1 GHz, $\lambda=0.3\text{m}$, $H_t=3\text{m}$, $U=20\text{m/s}$, $\sigma_{ht}=2.13\text{m}$, $\rho_c=102.6\text{m}$, $N_p=512$, $\Delta x=0.88\text{m}$, $X_{max}=450\text{m}$

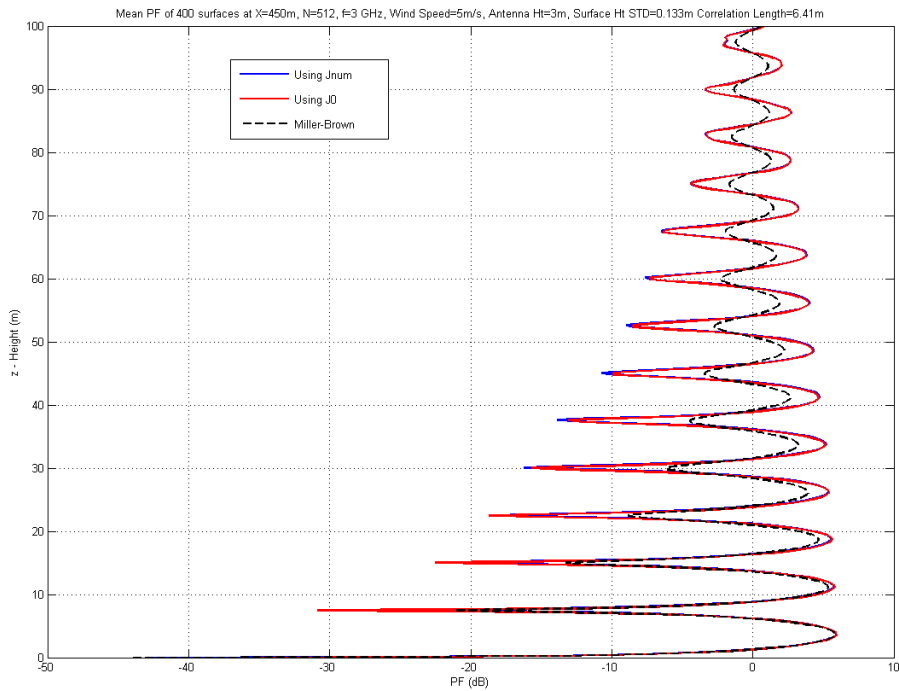


Figure 15: Monte-Carlo mean signal PF of 400 surface realizations at 3 GHz, $\lambda=0.1\text{m}$, $H_t=3\text{m}$, $U=5\text{m/s}$, $\sigma_{ht}=0.13\text{m}$, $\rho_c=6.41\text{m}$, $N_p=512$, $\Delta x=0.88\text{m}$, $X_{max}=450\text{m}$

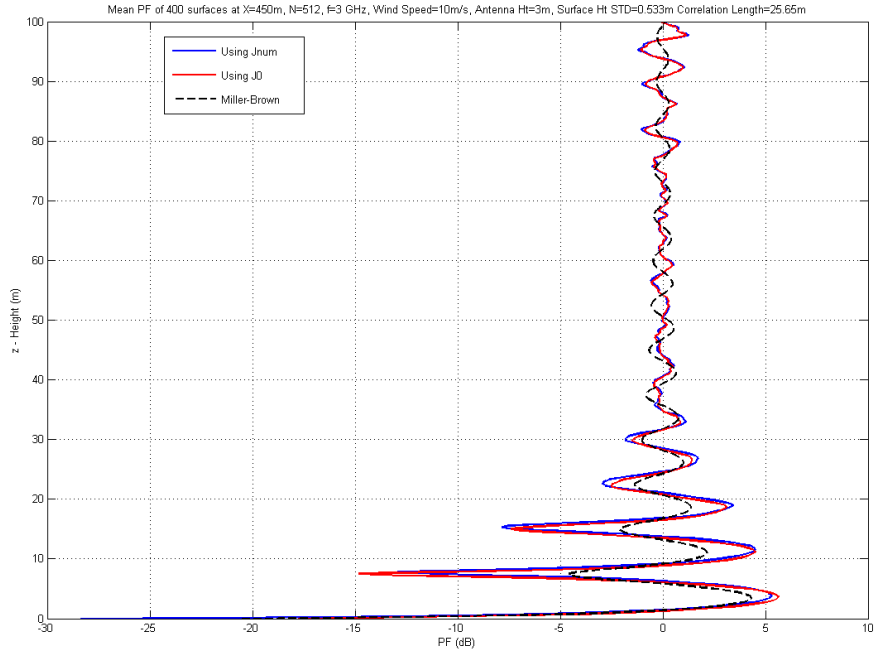


Figure 16: Monte-Carlo mean signal PF of 400 surface realizations at 3 GHz, $\lambda=0.1\text{m}$, $H_t=3\text{m}$, $U=10\text{m/s}$, $\sigma_h=0.53\text{m}$, $\rho_c=25.6\text{m}$, $N_p=512$, $\Delta x=0.88\text{m}$, $X_{max}=450\text{m}$

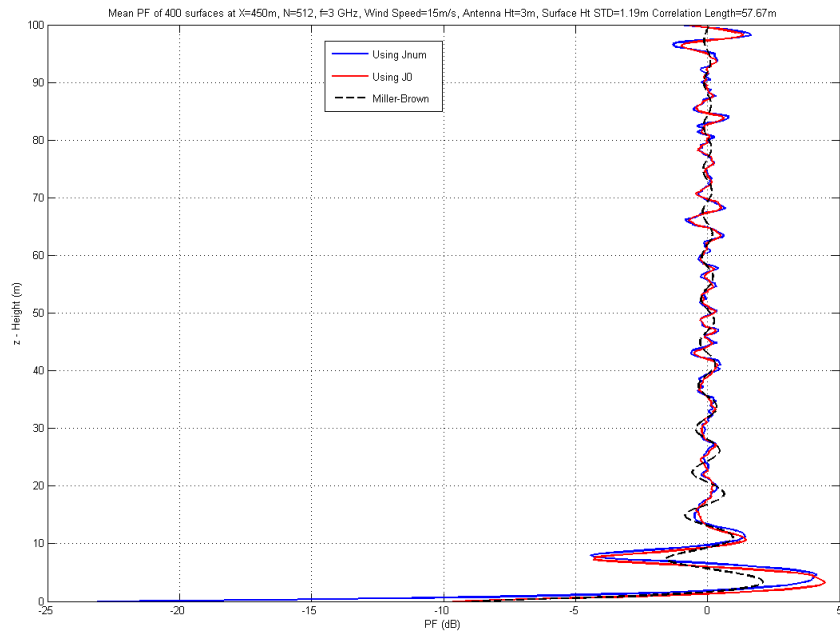


Figure 17: Monte-Carlo mean signal PF of 400 surface realizations at 3 GHz, $\lambda=0.1\text{m}$, $H_t=3\text{m}$, $U=15\text{m/s}$, $\sigma_h=1.19\text{m}$, $\rho_c=57.73\text{m}$, $N_p=512$, $\Delta x=0.88\text{m}$, $X_{max}=450\text{m}$

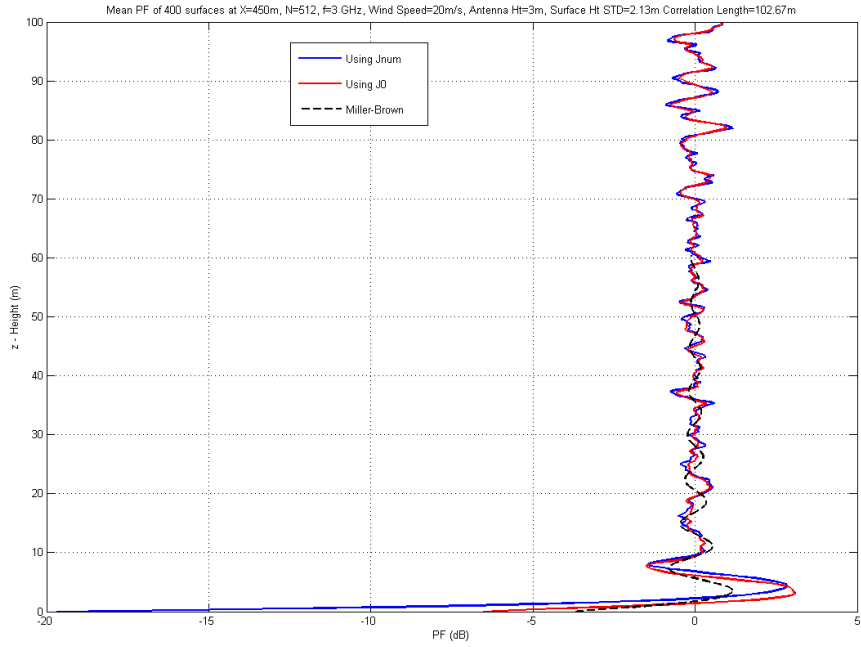


Figure 18: Monte-Carlo mean signal PF of 400 surface realizations at 3 GHz, $\lambda=0.1\text{m}$, $H_r=3\text{m}$, $U=20\text{m/s}$, $\sigma_h=2.13\text{m}$, $\rho_c=102.6\text{m}$, $N_p=512$, $\Delta x=0.88\text{m}$, $X_{max}=450\text{m}$

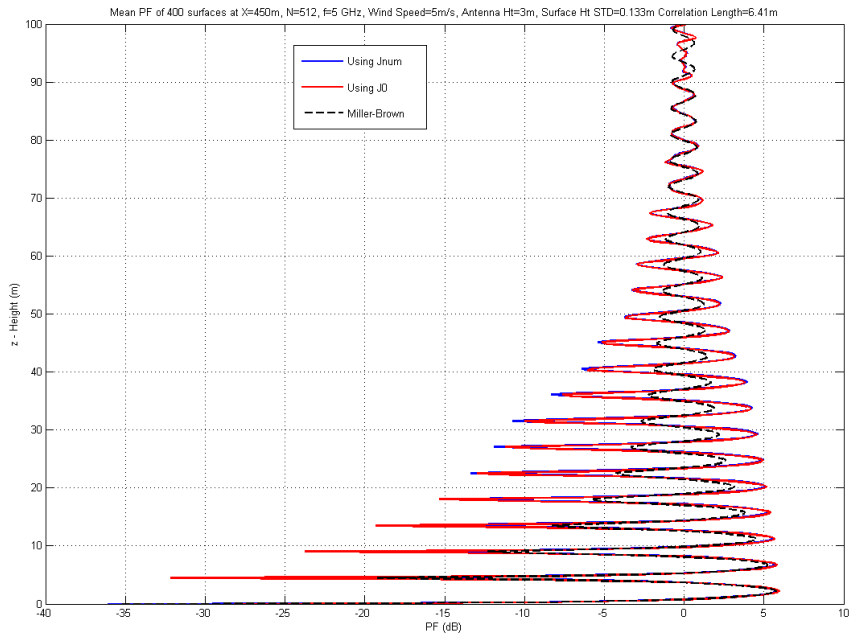


Figure 19: Monte-Carlo mean signal PF of 400 surface realizations at 5 GHz, $\lambda=0.06\text{m}$, $H_r=3\text{m}$, $U=5\text{m/s}$, $\sigma_h=0.13\text{m}$, $\rho_c=6.41\text{m}$, $N_p=512$, $\Delta x=0.88\text{m}$, $X_{max}=450\text{m}$

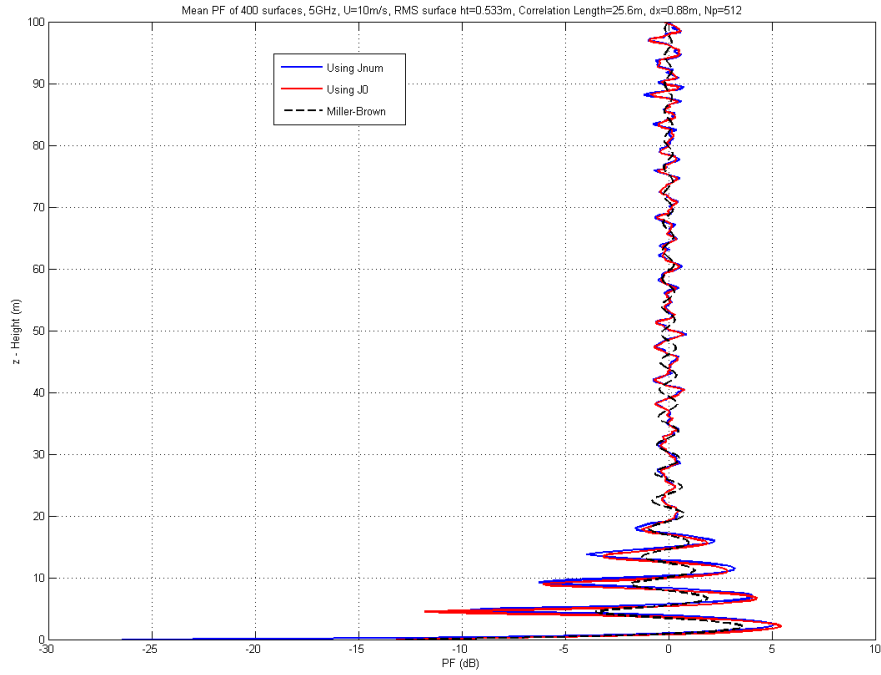


Figure 20: Monte-Carlo mean signal PF of 400 surface realizations at 5 GHz, $\lambda=0.06\text{m}$, $H_r=3\text{m}$, $U=10\text{m/s}$, $\sigma_h=0.53\text{m}$, $\rho_c=25.6\text{m}$, $N_p=512$, $\Delta x=0.88\text{m}$, $X_{max}=450\text{m}$

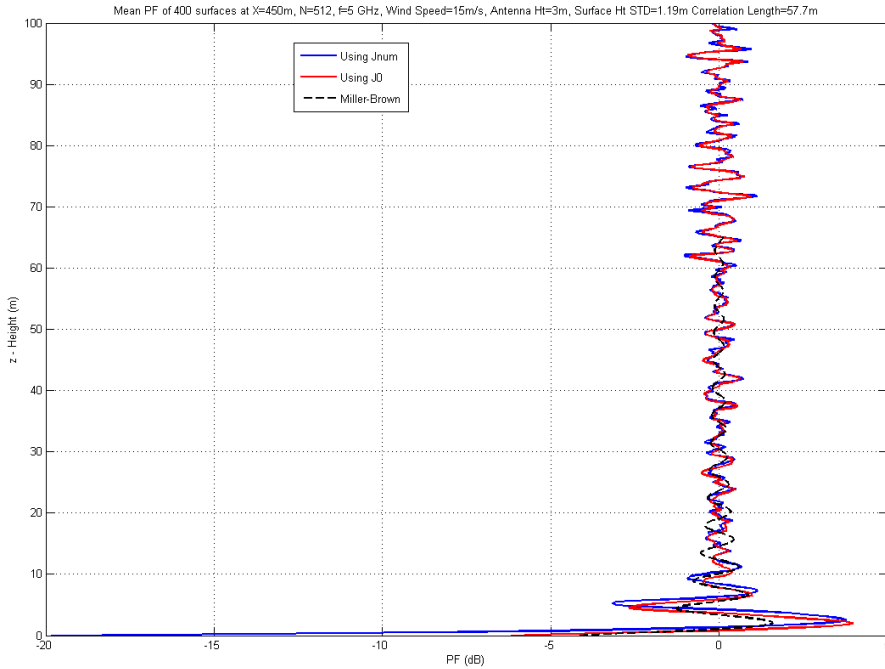


Figure 21: Monte-Carlo mean signal PF of 400 surface realizations at 5 GHz, $\lambda=0.06\text{m}$, $H_r=3\text{m}$, $U=15\text{m/s}$, $\sigma_h=1.19\text{m}$, $\rho_c=57.7\text{m}$, $N_p=512$, $\Delta x=0.88\text{m}$, $X_{max}=450\text{m}$

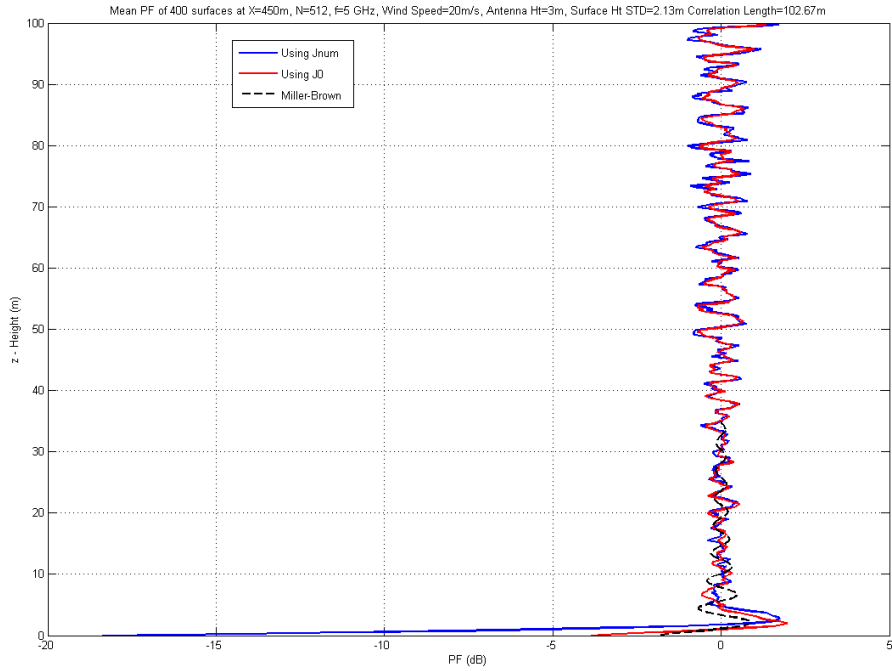


Figure 22: Monte-Carlo mean signal PF of 400 surface realizations at 5 GHz, $\lambda=0.06\text{m}$, $H_t=3\text{m}$, $U=20\text{m/s}$, $\sigma_h=2.13\text{m}$, $\rho_c=102.67\text{m}$, $N_p=512$, $\Delta x=0.88\text{m}$, $X_{max}=450\text{m}$

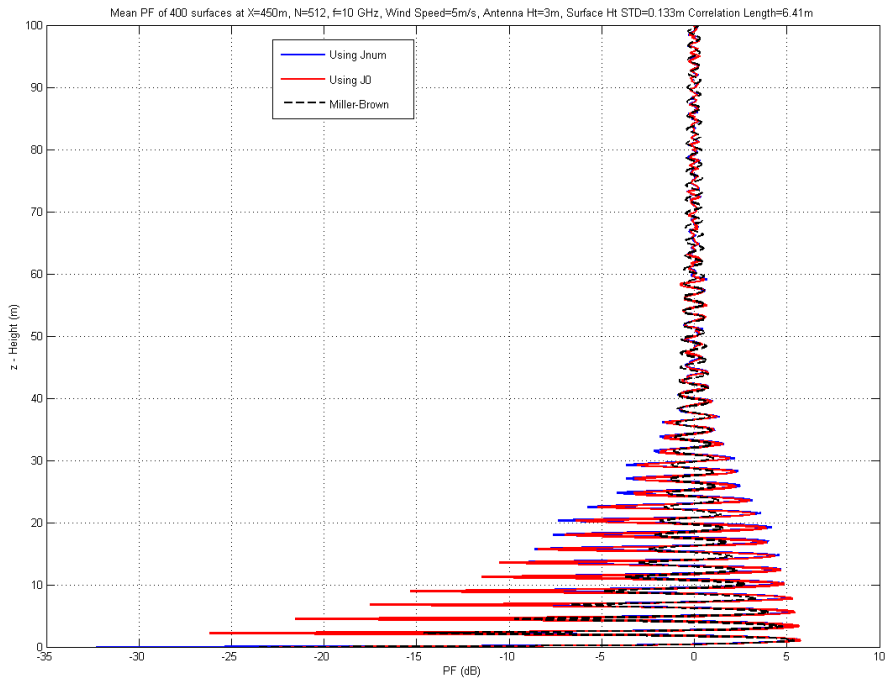


Figure 23: Monte-Carlo mean signal PF of 400 surface realizations at 10 GHz, $\lambda=0.03\text{m}$, $H_t=3\text{m}$, $U=5\text{m/s}$, $\sigma_h=0.13\text{m}$, $\rho_c=6.41\text{m}$, $N_p=512$, $\Delta x=0.88\text{m}$, $X_{max}=450\text{m}$

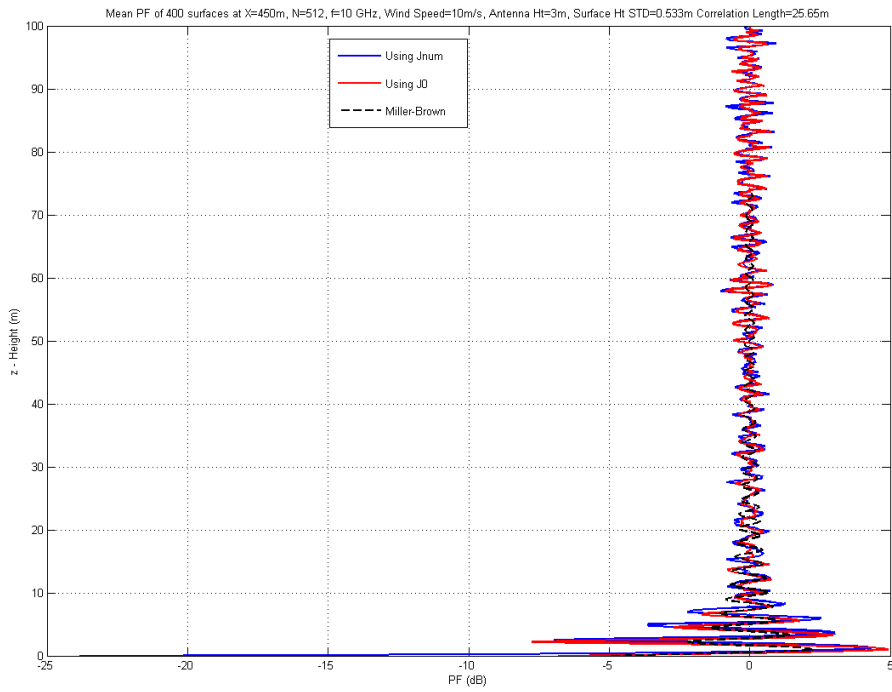


Figure 24: Monte-Carlo mean signal PF of 400 surface realizations at 10 GHz, $\lambda=0.03\text{m}$, $H_t=3\text{m}$, $U=10\text{m/s}$, $\sigma_h=0.53\text{m}$, $\rho_c=25.6\text{m}$, $N_p=512$, $\Delta x=0.88\text{m}$, $X_{max}=450\text{m}$

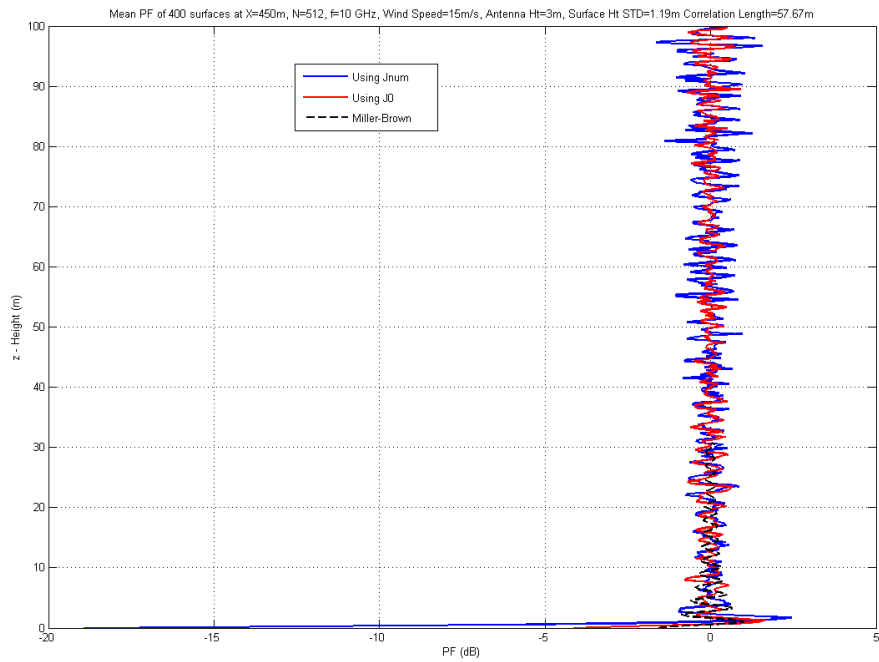


Figure 25: Monte-Carlo mean signal PF of 400 surface realizations at 10 GHz, $\lambda=0.03\text{m}$, $H_t=3\text{m}$, $U=15\text{m/s}$, $\sigma_h=1.19\text{m}$, $\rho_c=57.7\text{m}$, $N_p=512$, $\Delta x=0.88\text{m}$, $X_{max}=450\text{m}$

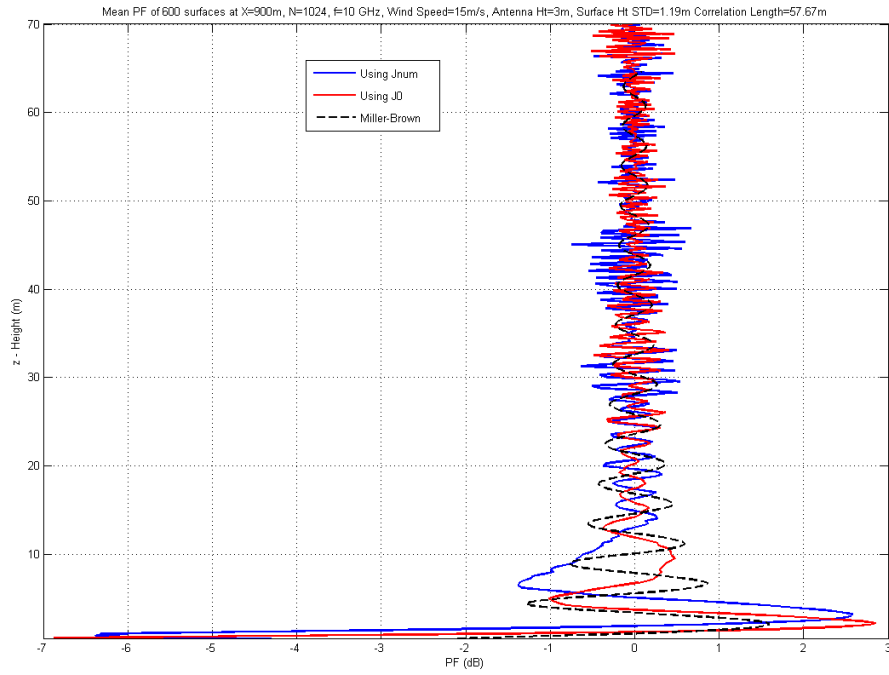


Figure 26: Monte-Carlo mean signal PF of 600 surface realizations at 10 GHz, $\lambda=0.03\text{m}$, $H_r=3\text{m}$, $U=15\text{m/s}$, $\sigma_h=1.19\text{m}$, $\rho_c=57.7\text{m}$, $N_p=512$, $\Delta x=0.88\text{m}$, $X_{max}=900\text{m}$

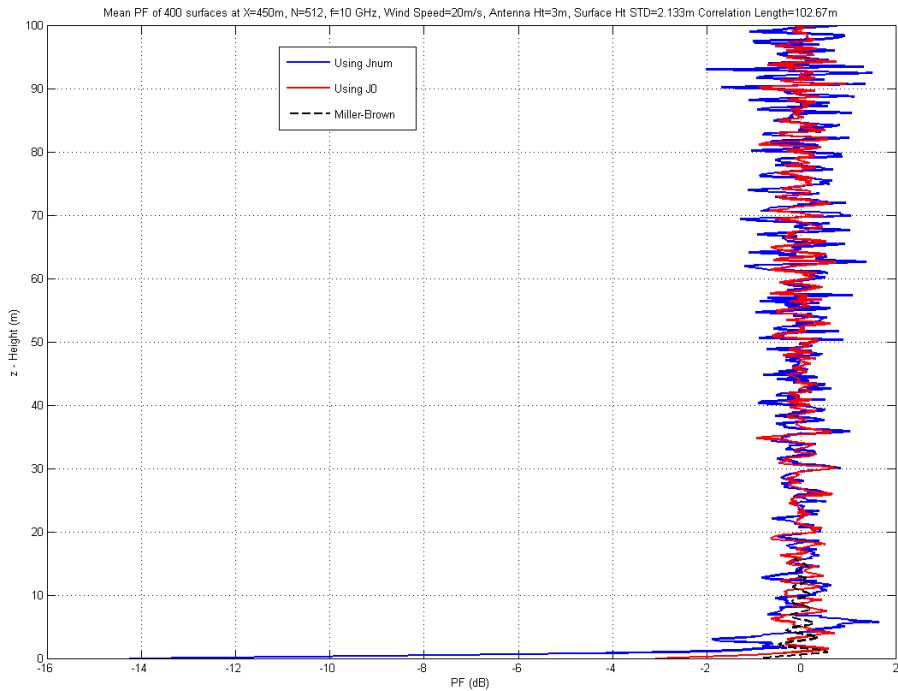


Figure 27: Monte-Carlo mean signal PF of 400 surface realizations at 10 GHz, $\lambda=0.03\text{m}$, $H_r=3\text{m}$, $U=20\text{m/s}$, $\sigma_h=2.13\text{m}$, $\rho_c=102.67\text{m}$, $N_p=512$, $\Delta x=0.88\text{m}$, $X_{max}=450\text{m}$

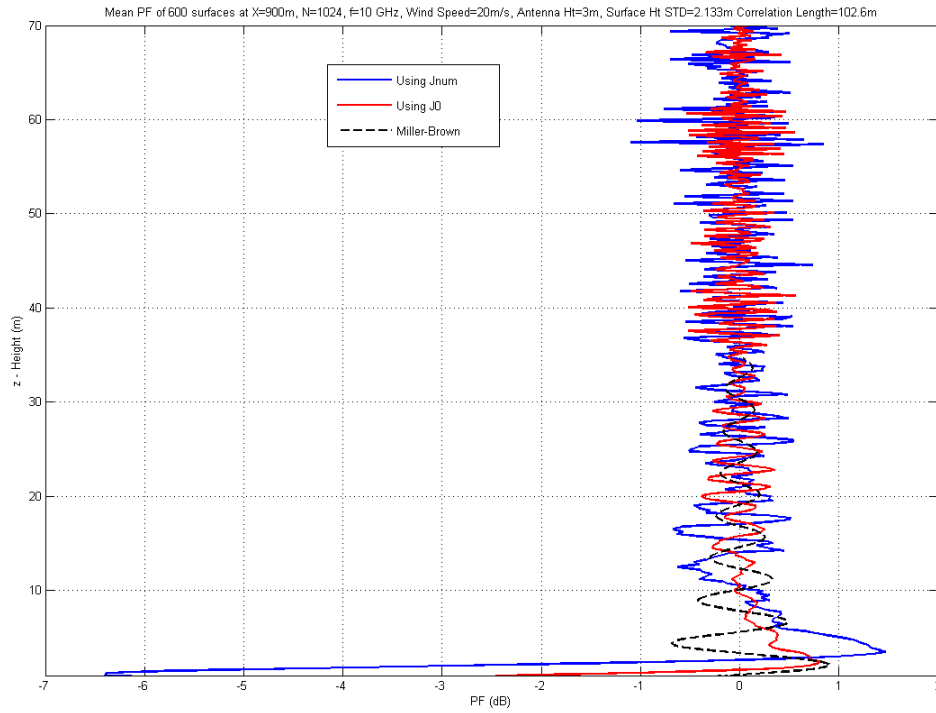


Figure 28: Monte-Carlo mean signal PF of 600 surface realizations at 10 GHz, $\lambda=0.03\text{m}$, $H_r=3\text{m}$, $U=20\text{m/s}$, $\sigma_h=2.13\text{m}$, $\rho_c=102.67\text{m}$, $N_p=512$, $\Delta x=0.88\text{m}$, $X_{max}=900\text{m}$

Wind Speed	σ_h/λ	φ_{mean} (deg)	No. of Nulls < -3dB (N_L)	φ_{mean}/N_L
1 GHz (L-band)				
5m/s	0.44	0.85	5	0.17
10m/s	1.77	1.6	3	0.53
15m/s	3.96	1.35	2	0.68
20m/s	7.1	1.06	1	1.06
3 GHz (S-band)				
5m/s	1.33	1.78	13	0.14
10m/s	5.33	1.9	3	0.63
15m/s	11.99	1.41	2	0.71
20m/s	21.33	1.15	1	1.15
5 GHz (C-band)				
5m/s	2.21	2.2	14	0.16
10m/s	8.88	1.86	4	0.47
15m/s	19.98	1.44	2	0.72
20m/s	35.55	1.24	1	1.24

Wind Speed	σ_h/λ	φ_{mean} (deg)	No. of Nulls < -3dB (N_L)	φ_{mean}/N_L
10 GHz (X-band)				
5m/s	4.43	2.33	14	0.17
10m/s	17.76	1.96	3	0.65
15m/s	39.96	2.3	1	2.30
20m/s	71.1	2.6	1	2.60

Table 1: Monte Carlo Mean Signal PF at different frequencies and roughness at $X_{max} = 450m$

It can be observed that as the frequency increases, the number of nulls in the interference pattern of the PF also increases at lower wind speeds and the agreement between the mean PF computed using J_{num} and J_0 is best at a speed of 5m/s at all frequencies in consideration. Also, at large heights, for e.g. beyond 70m in the 3 GHz-20m/s (Figure 18) and 5 GHz-20 m/s (Figure 22) case, the scattered field gets larger and exhibits noisy interference pattern. Based on these results, a subjective threshold value of $\frac{\varphi_{mean}}{N_L} \sim \leq 1^\circ$ and $\sigma_h \leq 20\lambda$ is determined where the Monte-Carlo zeroth order solution seems to have reasonably good agreement with the Monte-Carlo exact solution (cases highlighted in green in Table 1). At 10 GHz and wind speeds of 5m/s and 10m/s (Figure 23 and Figure 24 respectively), the agreement is good, but at 15m/s (Figures 25, 26) and 20m/s (Figures 27, 28), the PF shows noisy pattern, which may be attributed to the following reasons:

1. Since the Monte-Carlo solution error convergence rate is inversely proportional to the square root of number of realizations, the current number of realizations (i.e. 400 surfaces) may not be adequate.
2. Limitations on the accuracy of number of significant digits that can be processed by the software (i.e. Matlab in this case) running the computation.
3. The diffused components of the scattered field are significantly high that any meaningful interference pattern cannot be visualized.

In order to verify that the phase of the integrand in Eq. 3.2.2 corresponding to the zeroth order current density is accurately sampled with respect to the integration variable theta (θ), the unwrapped phase (in degrees) of the integrand is plotted against theta (θ) at two

different values of $x = 111.8\text{m}$ and 450m for a wind-speed of 10m/s and an incident radio-wave frequency of 10 GHz . The figures are shown below:

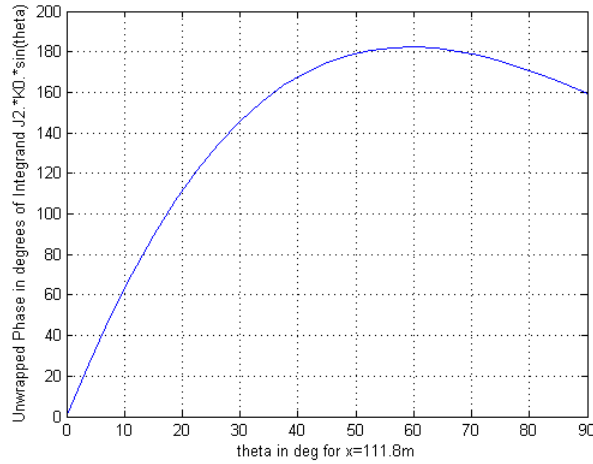


Figure 29: Phase of integrand for J0 solution w.r.t. integration variable at $x=111.8\text{m}$

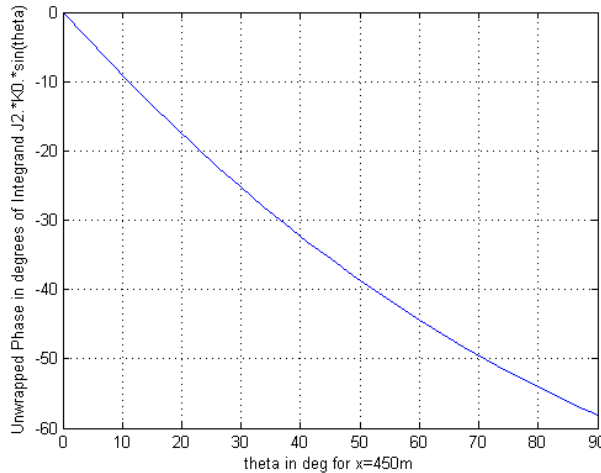


Figure 30: Phase of integrand for J0 solution w.r.t. integration variable at $x=450\text{m}$

The maximum phase difference between two successive points of the integrand is less than about 19° at 10 GHz , which shows that the zeroth order solution is numerically well computed with adequate phase sampling.

A plot of magnitude of J_{num} and J_0 (Figure 31, Figure 32) as well as the phase (Figure 33, Figure 34) overlay on a single realization of rough surface in comparison with its slope and curvature shows that at 10 GHz , the agreement between J_{num} and J_0 (both magnitude and phase) is better at 5m/s than at 10m/s . This gives an exact picture of the current distribution over the rough surface and its variations in the peaks and troughs.

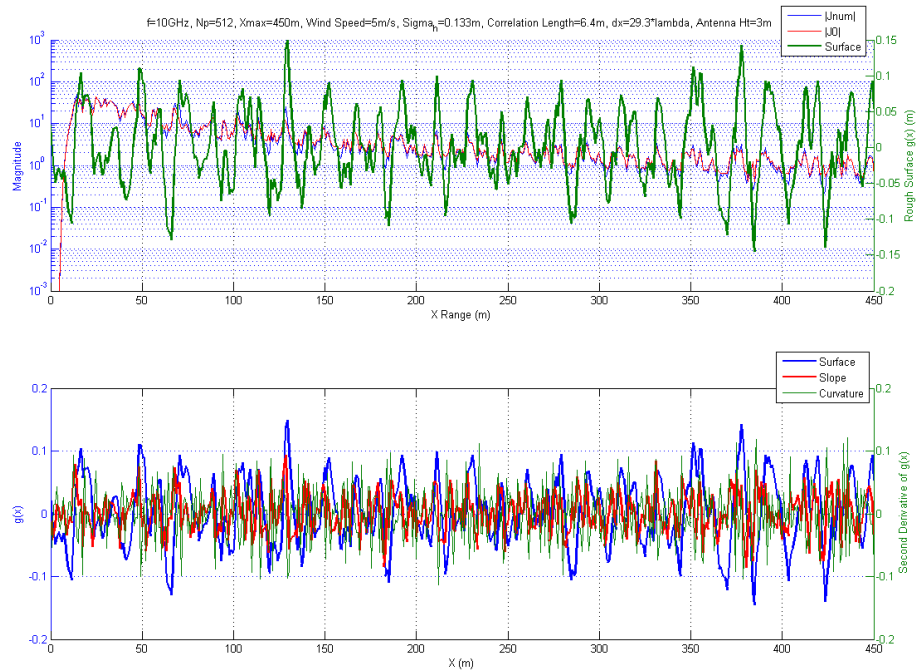


Figure 31: Overlay of surface with $|J_{num}|$ and $|J_0|$ at 10 GHz, 5m/s

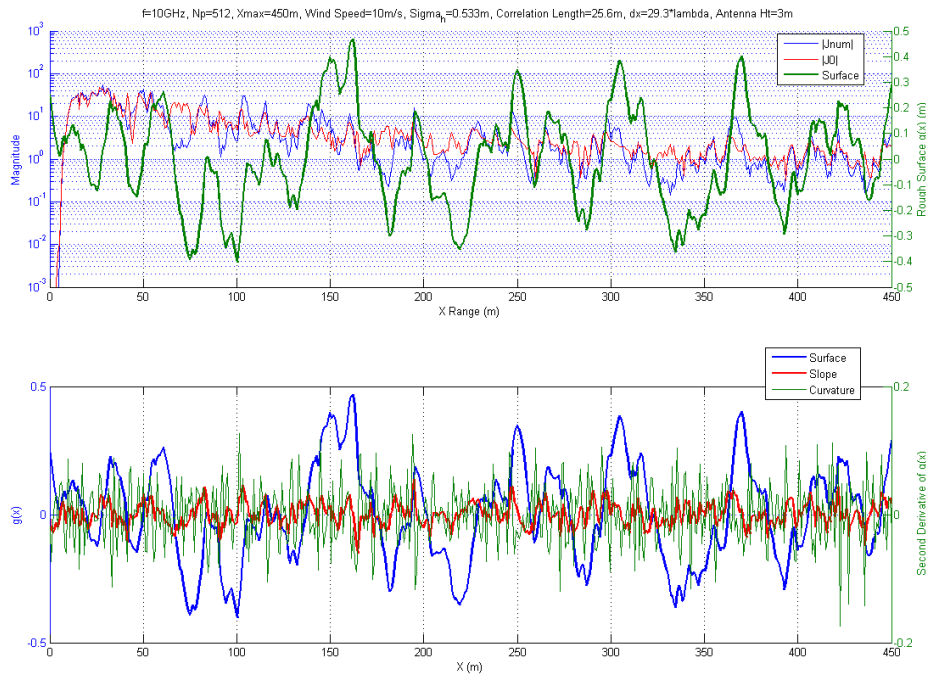


Figure 32: Overlay of surface with $|J_{num}|$ and $|J_0|$ at 10 GHz, 10m/s

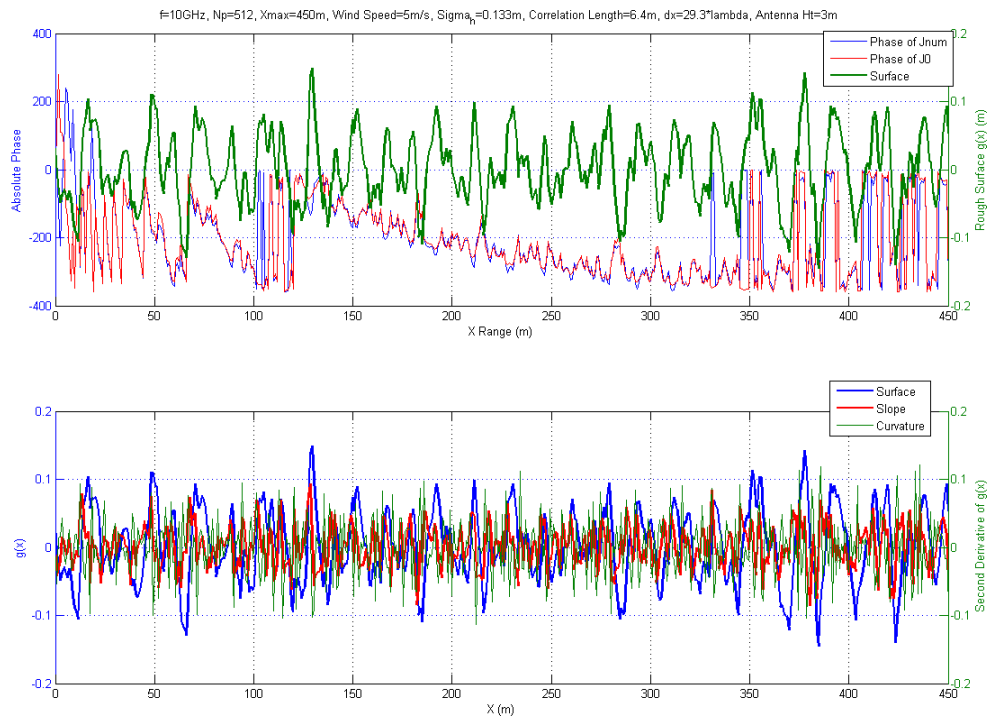


Figure 33: Overlay of surface with Phase of Jnum and J0 at 10 GHz, 5m/s

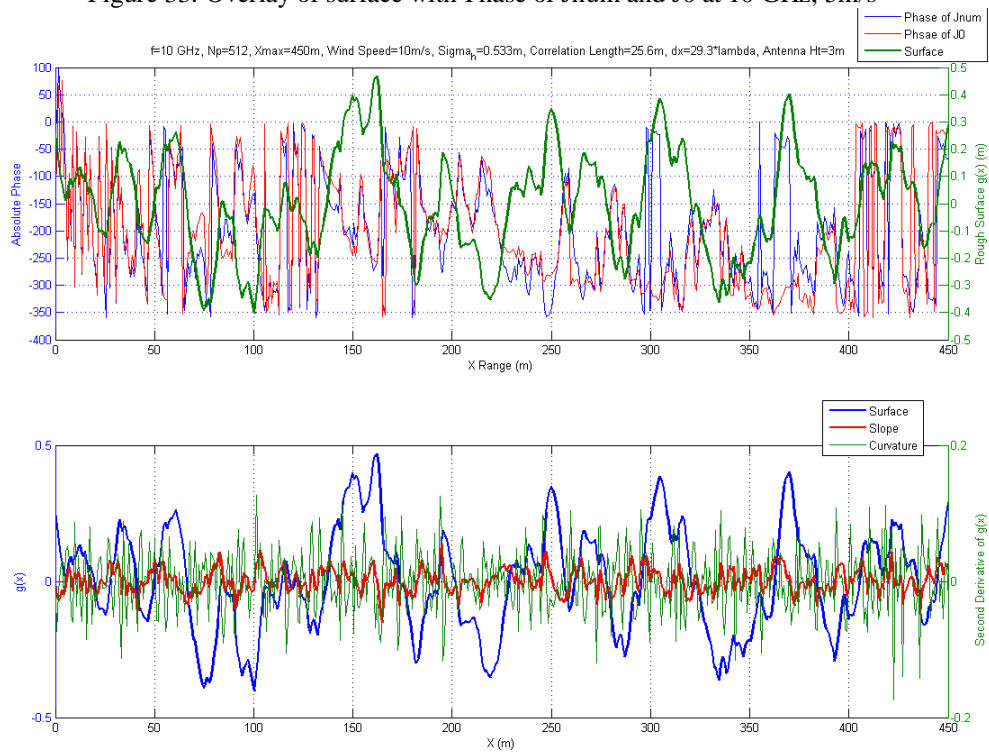


Figure 34: Overlay of surface with Phase of Jnum and J0 at 10 GHz, 10m/s

5.2. Mean Power PF using Monte-Carlo simulations

The mean signal propagation factor takes into account the phase of the scattered field for each surface realization, which is then averaged over many realizations using Monte-Carlo simulations. In case of power PF, the phase information in the scattered field is not considered since the square magnitude of the scattered field is averaged over many surface realizations. Hence, this PF can also be known as *non-coherent power PF* and is given as $Power\ PF = 10 \log_{10} \left\{ \left\langle \left| \frac{U_s + U_{inc}}{U_{inc}} \right|^2 \right\rangle \right\}$. Thus for a single realization of the surface, the squared absolute scattered field is considered and then averaged over many surface realizations.

If we denote the power scattered from the surface as P_s , then $P_s = |U_s|^2$ and the mean power PF can be expressed as:

$$Mean\ Power\ PF = 10 * \log_{10} \left[1 + \frac{\langle P_s \rangle}{|U_{inc}|^2} + 2 * Real \left(\frac{\langle U_s \rangle}{U_i} \right) \right] \quad Eq. 5.2.1$$

In order to provide a comparison with a known analytical solution to the mean scattered power, Kirchhoff's approximation method for a Gaussian spectrum as outlined in Beckmann ^[16] has been used as reference. For this, a rough surface with Gaussian spectrum and Gaussian height statistics is used.

From Eq. 4.1.12 for the incident field, one of the exponent terms of the integrand is $e^{-ik_z^2 x / 2k_0}$ which is the only factor governing the incident field as a function of x . Let us denote $k_x = \sqrt{k_0^2 - k_z^2}$. Then,

$$\frac{k_z^2}{2k_0} = k_0 - \sqrt{k_0^2 - k_z^2} \quad Eq. 5.2.2$$

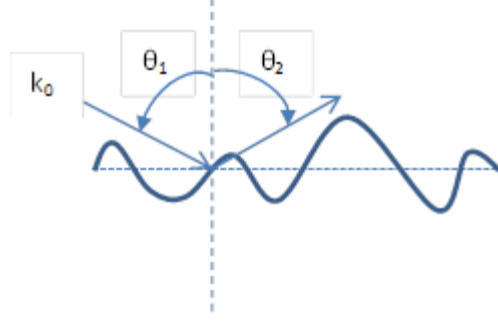


Figure 35: Schematic depicting the propagation of radio-waves and angle of incidence, reflection according to Beckmann

Since the incident wave is hitting the rough surface in the direction shown at an angle θ_1 taken anti-clockwise from the normal to the mean surface, we need to make a change of variable from k_z to $-k_z$, when we realize that the integrand actually represents a 2-D plane wave. $k_z = k_0 \cos \theta_1$ The amplitude of this plane wave would be $U_0(-k_z)$, which is the Fourier transform of the initial source field, but with a change of sign in k_z .

Using Eq. 5.2.2 in Eq. 4.1.12, we can rewrite the incident field as:

$$U_{inc}(x, z) = e^{ik_0 x} \int_{-\infty}^{\infty} U_0(-k_z) e^{-i(k_x x + k_z(z-g_0))} dk_z \quad \text{Eq. 5.2.3}$$

We multiply the amplitude of the plane wave i.e. $U_0(-k_z)$ with E_{20} , which is the specular scattered field from a perfectly smooth flat PEC surface for the same incidence, source field strength, same distance and surface dimensions as the rough surface. Let us denote the scattered field from a rough surface as E_2 . The Kirchhoff's scattering co-efficient is then given as $\rho = \frac{E_2}{E_{20}}$

The mean scattered power is given by:

$$\text{Mean Scattered Power} = |E_{20}|^2 * \langle \rho \rho^* \rangle \quad \text{Eq. 5.2.4}$$

where from ^[16],

$$E_{20} = \frac{-ik_z e^{ik_0 R_0} U_0(-k_z) X_{max}}{\pi R_0} \quad \text{Eq. 5.2.5}$$

The quantity R_0 is the distance of the observation point along the vertical z line from the origin. Note that E_{20} represents the scattered field outside the region encompassing

scattering surface, which is assumed to lie between $(0, X_{max})$. Hence, there is no problem that E_{20} goes to zero in the far-zone outside $(0, X_{max})$.

$$\langle \rho \rho^* \rangle = \left[\rho_0^2 + \frac{\sqrt{\pi} F^2 T}{X_{max}} \sum_{m=1}^{\infty} \frac{g^m}{m! \sqrt{m}} e^{-v_x^2 T^2 / 4m} \right] e^{-g} \quad \text{Eq. 5.2.6}$$

The parameters in the above equation are defined as follows:

$$\rho_0 = \text{sinc} \left(\frac{v_x X_{max}}{2} \right) \quad \text{Eq. 5.2.7}$$

$$v_x = k_0 (\sin \theta_1 - \sin \theta_2) \quad \text{Eq. 5.2.8}$$

$$F = \sec(\theta_1) \frac{1 + \cos(\theta_1 + \theta_2)}{\cos \theta_1 + \cos \theta_2} \quad \text{Eq. 5.2.9}$$

$$g = \left\{ \frac{2\pi\sigma}{\lambda} (\cos \theta_1 + \cos \theta_2) \right\}^2 \quad \text{Eq. 5.2.10}$$

The parameter T is the same as ρ_c in case of PM spectrum; the correlation length of the surface. In our case, we consider a Gaussian surface at 3GHz, with RMS surface height $\sigma = 1.19\text{m}$ and $T = 57.7\text{m}$, $X_{max} = 450\text{m}$.

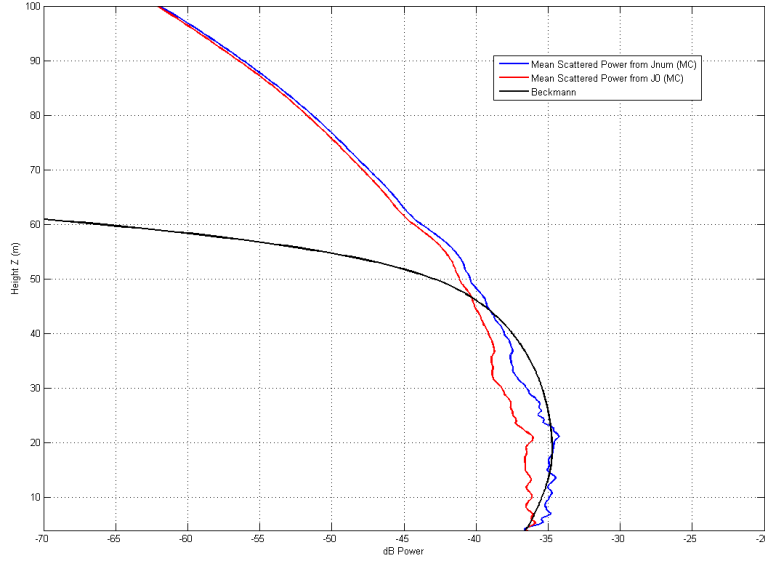


Figure 36: Comparison of mean scattered power from Jnum, J0 of Monte-Carlo with Kirchhoff's solution outlined in Beckmann

The comparison with Kirchhoff's solution with Monte-Carlo mean scattered power at 3 GHz shows that the solutions are in good agreement, though the analytical Kirchhoff's

solution converges at about a height of 60 m compared to the Monte-Carlo method, it matches well with Monte-Carlo solution at low heights, closer to the surface.

As before, one representative mid-band frequency in each of 'L', 'S', 'C' and 'X' bands is considered and wind-speeds of 5m/s, 10m/s, 15 m/s and 20 m/s at each of these frequencies is analyzed for the mean power PF. The results have been presented below.

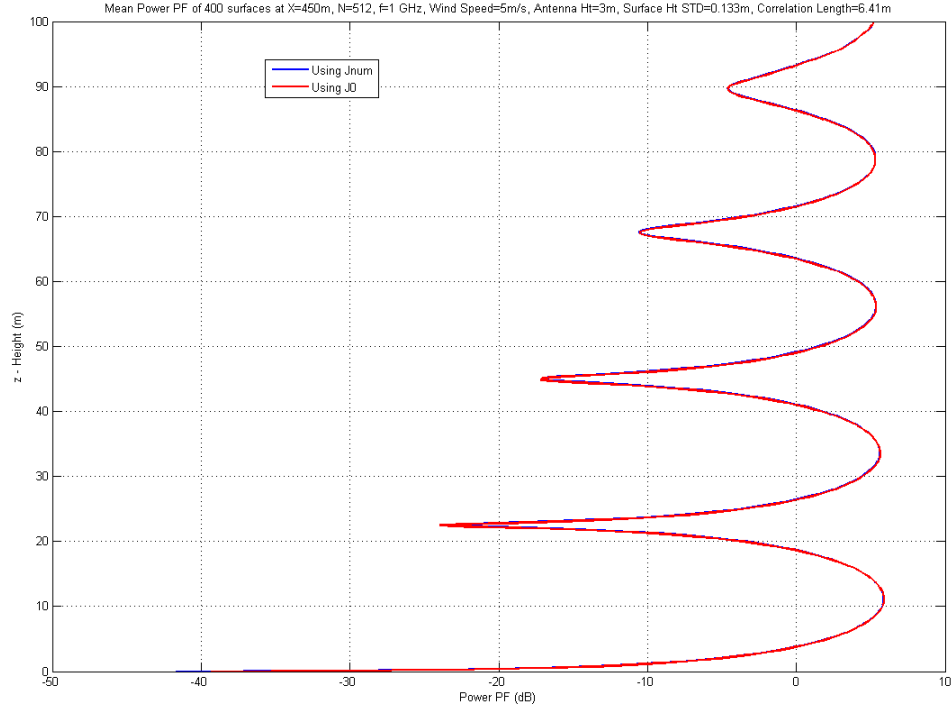


Figure 37: Monte-Carlo mean power PF of 400 surface realizations at 1 GHz, $\lambda=0.3\text{m}$, $H_t=3\text{m}$, $U=5\text{m/s}$, $\sigma_{ht}=0.13\text{m}$, $\rho_c=6.41\text{m}$, $N_p=512$, $\Delta x=0.88\text{m}$, $X_{max}=450\text{m}$

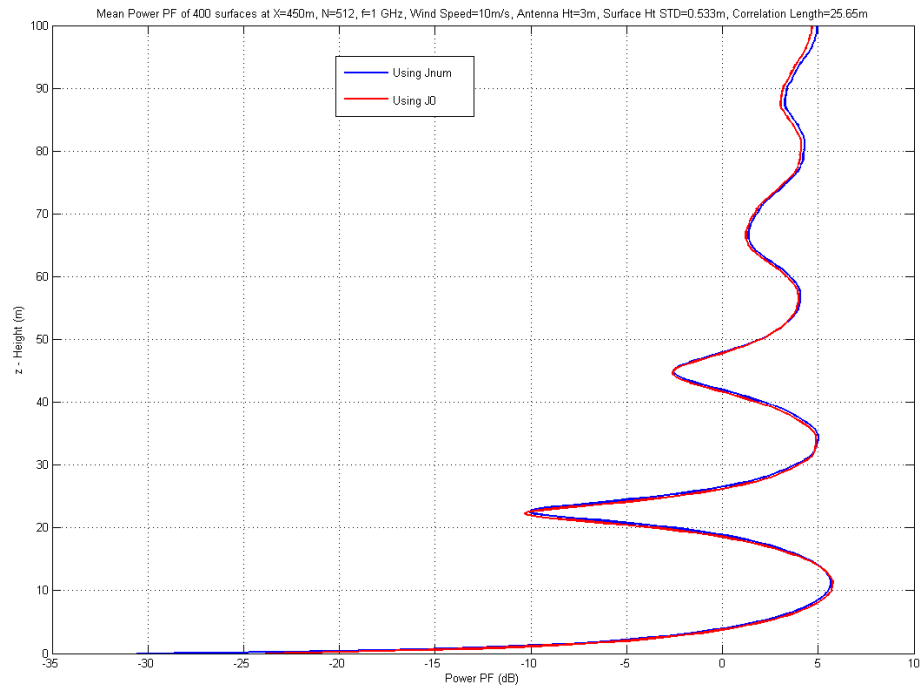


Figure 38: Monte-Carlo mean power PF of 400 surface realizations at 1 GHz, $\lambda=0.3\text{m}$, $H_t=3\text{m}$, $U=10\text{m/s}$, $\sigma_h=0.53\text{m}$, $\rho_c=25.6\text{m}$, $N_p=512$, $\Delta x=0.88\text{m}$, $X_{max}=450\text{m}$

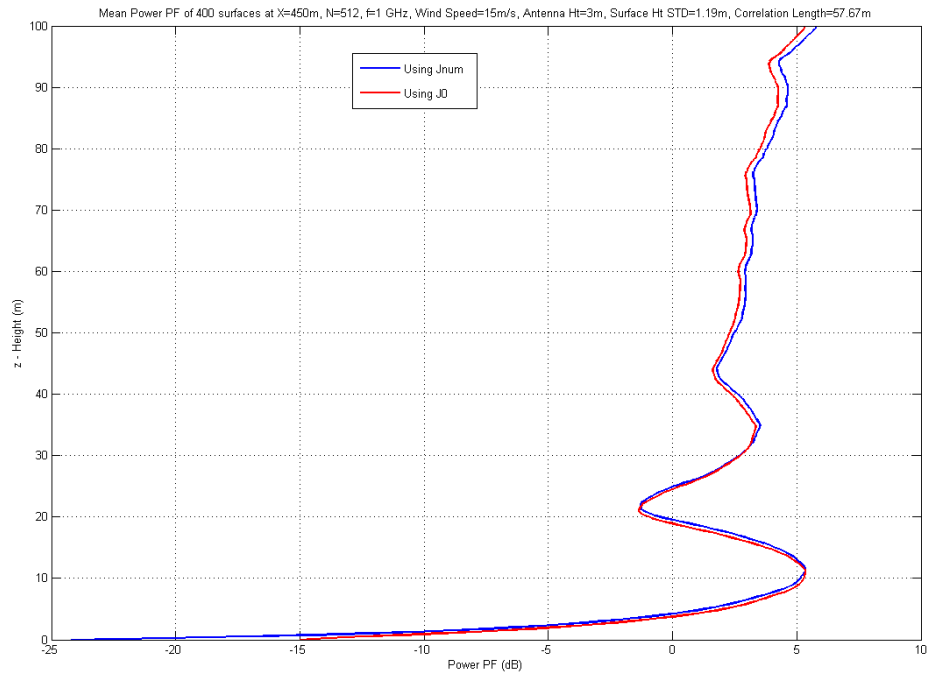


Figure 39: Monte-Carlo mean power PF of 400 surface realizations at 1 GHz, $\lambda=0.3\text{m}$, $H_t=3\text{m}$, $U=15\text{m/s}$, $\sigma_h=1.19\text{m}$, $\rho_c=57.73\text{m}$, $N_p=512$, $\Delta x=0.88\text{m}$, $X_{max}=450\text{m}$

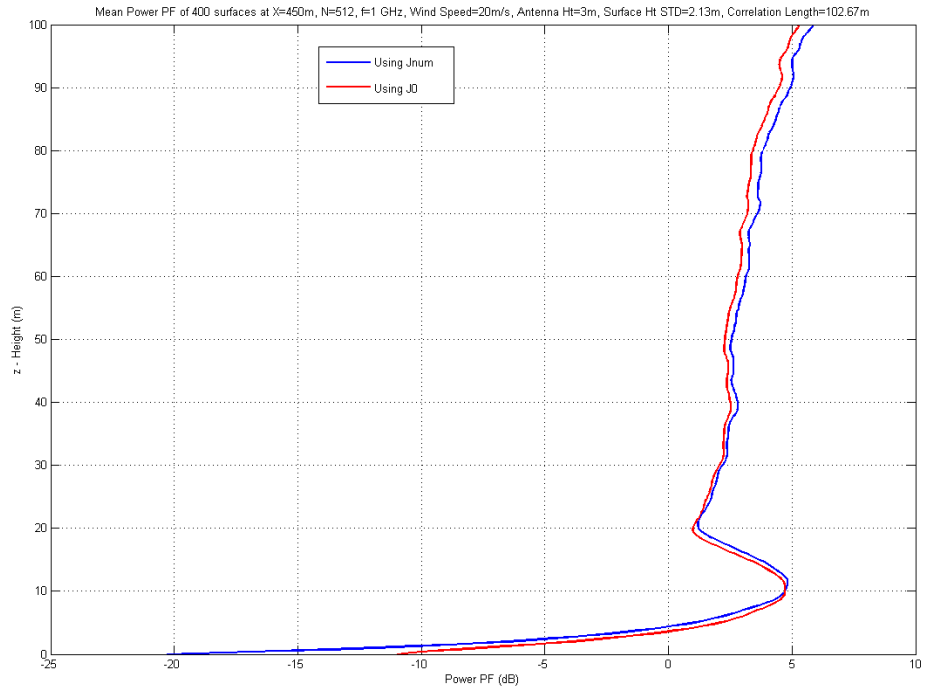


Figure 40: Monte-Carlo mean power PF of 400 surface realizations at 1 GHz, $\lambda=0.3\text{m}$, $H_t=3\text{m}$, $U=20\text{m/s}$, $\sigma_{ht}=2.13\text{m}$, $\rho_c=102.6\text{m}$, $N_p=512$, $\Delta x=0.88\text{m}$, $X_{max}=450\text{m}$

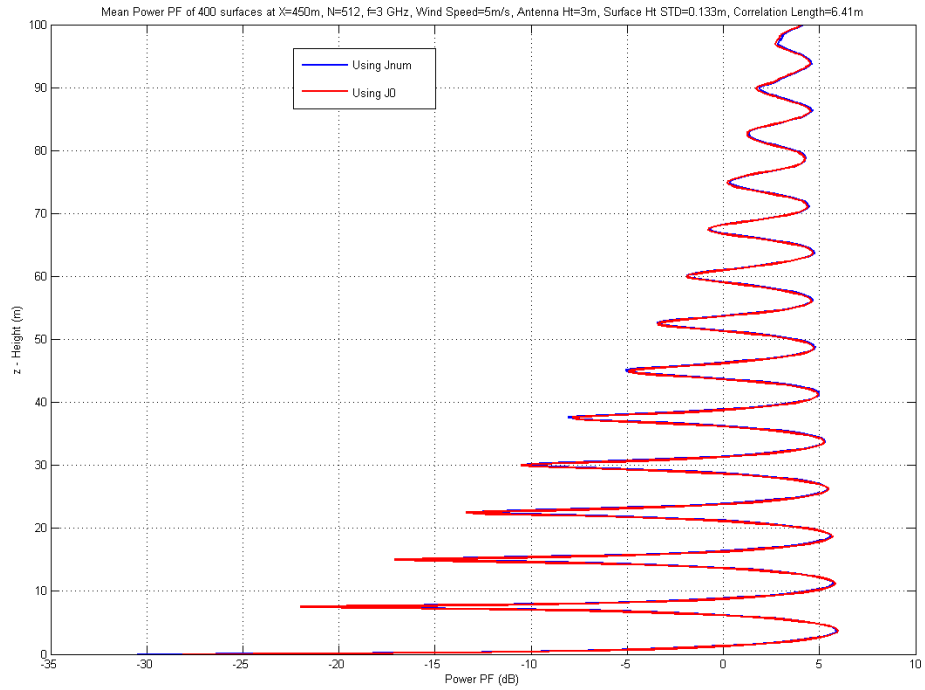


Figure 41: Monte-Carlo mean power PF of 400 surface realizations at 3 GHz, $\lambda=0.1\text{m}$, $H_t=3\text{m}$, $U=5\text{m/s}$, $\sigma_{ht}=0.13\text{m}$, $\rho_c=6.41\text{m}$, $N_p=512$, $\Delta x=0.88\text{m}$, $X_{max}=450\text{m}$

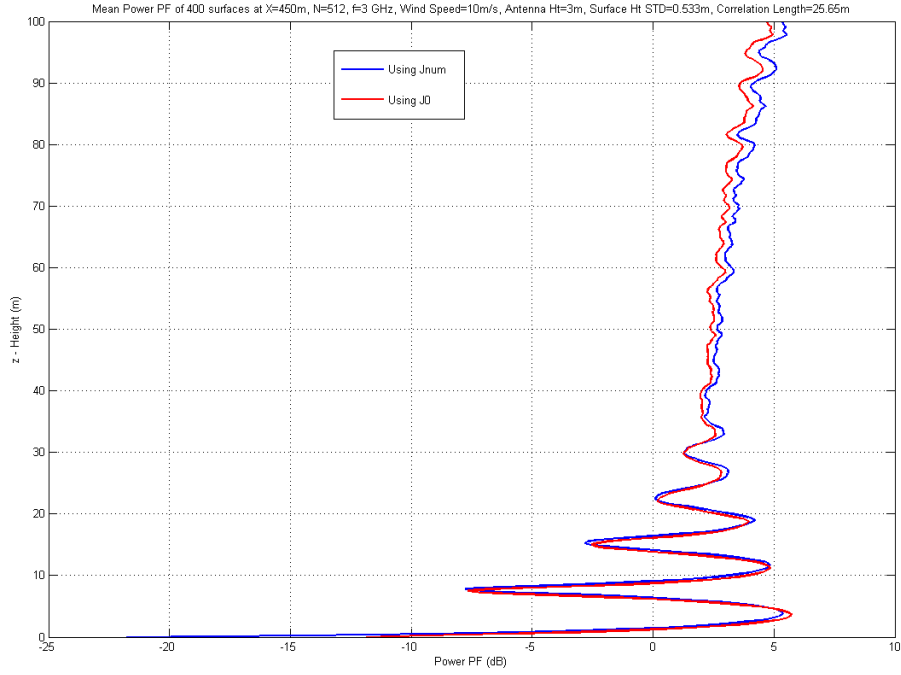


Figure 42: Monte-Carlo mean power PF of 400 surface realizations at 3 GHz, $\lambda=0.1\text{m}$, $H_t=3\text{m}$, $U=10\text{m/s}$, $\sigma_h=0.53\text{m}$, $\rho_c=25.6\text{m}$, $N_p=512$, $\Delta x=0.88\text{m}$, $X_{max}=450\text{m}$

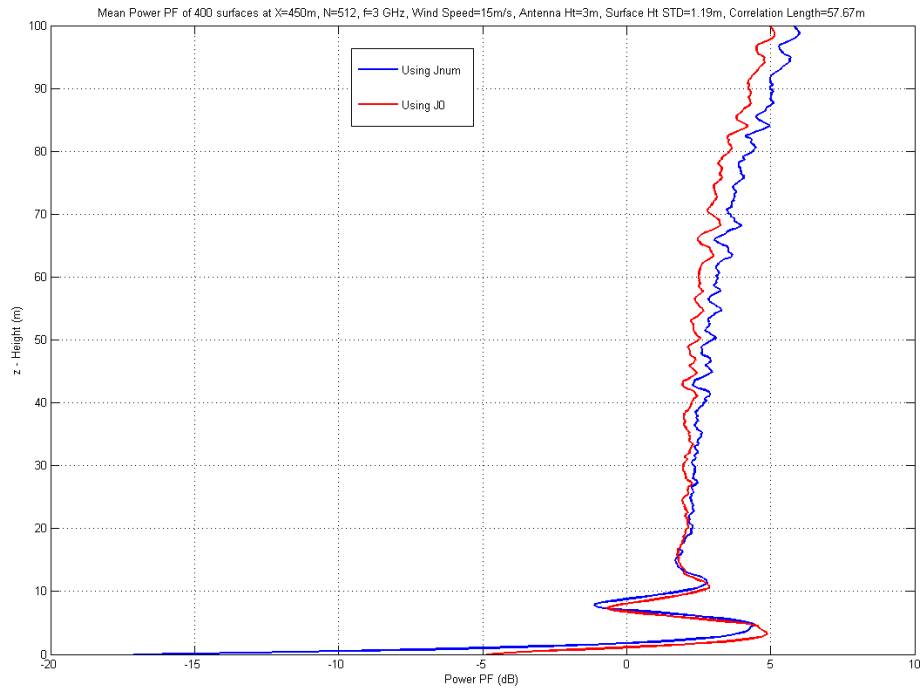


Figure 43: Monte-Carlo mean power PF of 400 surface realizations at 3 GHz, $\lambda=0.1\text{m}$, $H_t=3\text{m}$, $U=15\text{m/s}$, $\sigma_h=1.19\text{m}$, $\rho_c=57.73\text{m}$, $N_p=512$, $\Delta x=0.88\text{m}$, $X_{max}=450\text{m}$

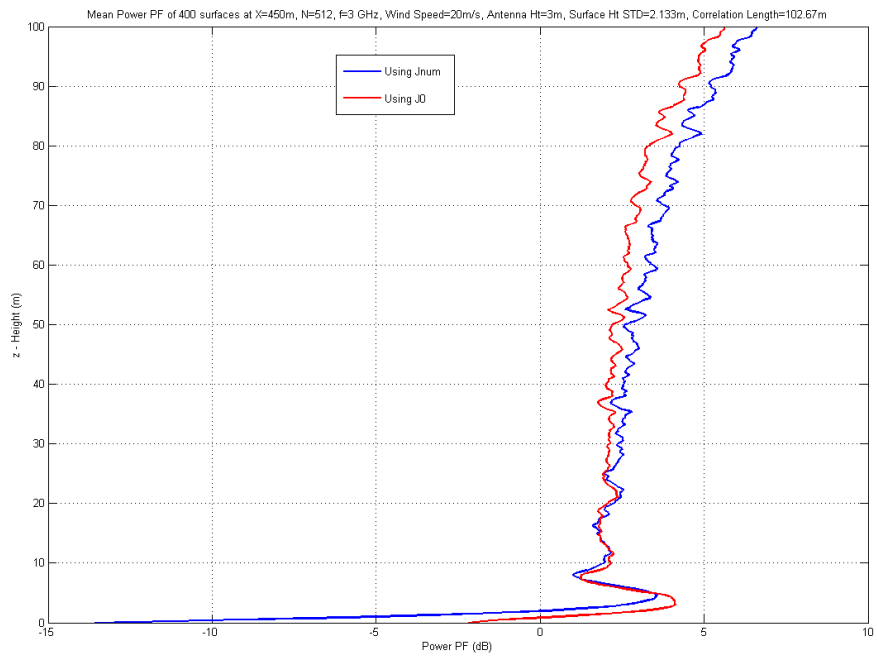


Figure 44: Monte-Carlo mean power PF of 400 surface realizations at 3 GHz, $\lambda=0.1\text{m}$, $H_t=3\text{m}$, $U=20\text{m/s}$, $\sigma_h=2.13\text{m}$, $\rho_c=102.6\text{m}$, $N_p=512$, $\Delta x=0.88\text{m}$, $X_{max}=450\text{m}$

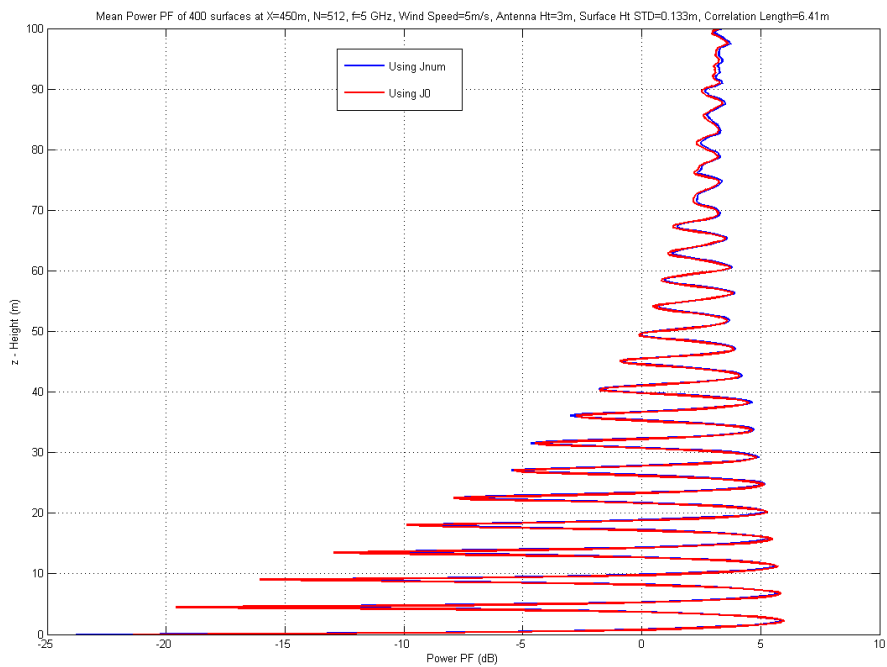


Figure 45: Monte-Carlo mean power PF of 400 surface realizations at 5 GHz, $\lambda=0.06\text{m}$, $H_t=3\text{m}$, $U=5\text{m/s}$, $\sigma_h=0.13\text{m}$, $\rho_c=6.41\text{m}$, $N_p=512$, $\Delta x=0.88\text{m}$, $X_{max}=450\text{m}$

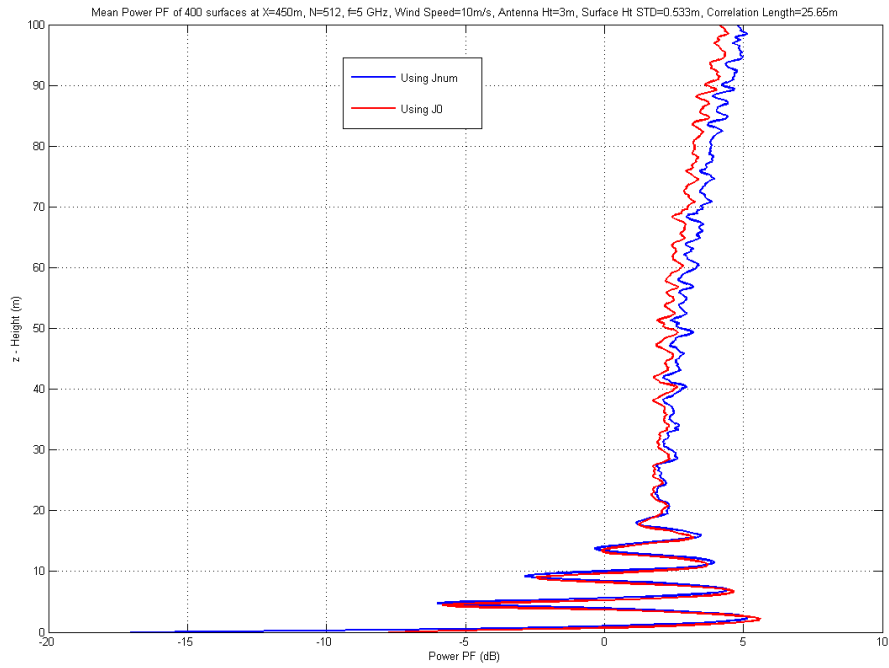


Figure 46: Monte-Carlo mean power PF of 400 surface realizations at 5 GHz, $\lambda=0.06\text{m}$, $H_t=3\text{m}$, $U=10\text{m/s}$, $\sigma_h=0.53\text{m}$, $\rho_c=25.6\text{m}$, $N_p=512$, $\Delta x=0.88\text{m}$, $X_{max}=450\text{m}$

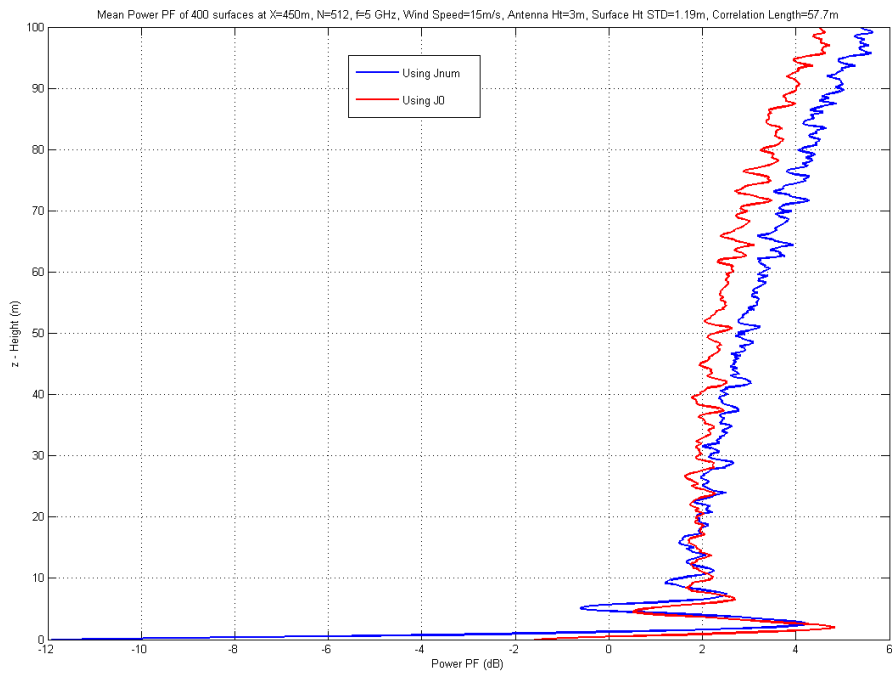


Figure 47: Monte-Carlo mean power PF of 400 surface realizations at 5 GHz, $\lambda=0.06\text{m}$, $H_t=3\text{m}$, $U=15\text{m/s}$, $\sigma_h=1.19\text{m}$, $\rho_c=57.73\text{m}$, $N_p=512$, $\Delta x=0.88\text{m}$, $X_{max}=450\text{m}$

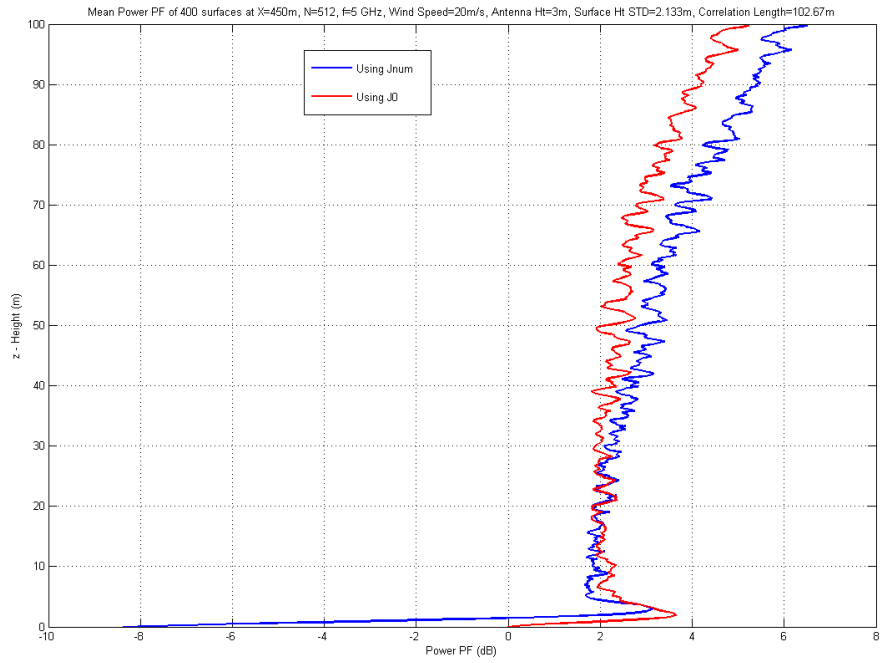


Figure 48: Monte-Carlo mean power PF of 400 surface realizations at 5 GHz, $\lambda=0.06\text{m}$, $H_t=3\text{m}$, $U=20\text{m/s}$, $\sigma_h=2.13\text{m}$, $\rho_c=102.6\text{m}$, $N_p=512$, $\Delta x=0.88\text{m}$, $X_{max}=450\text{m}$

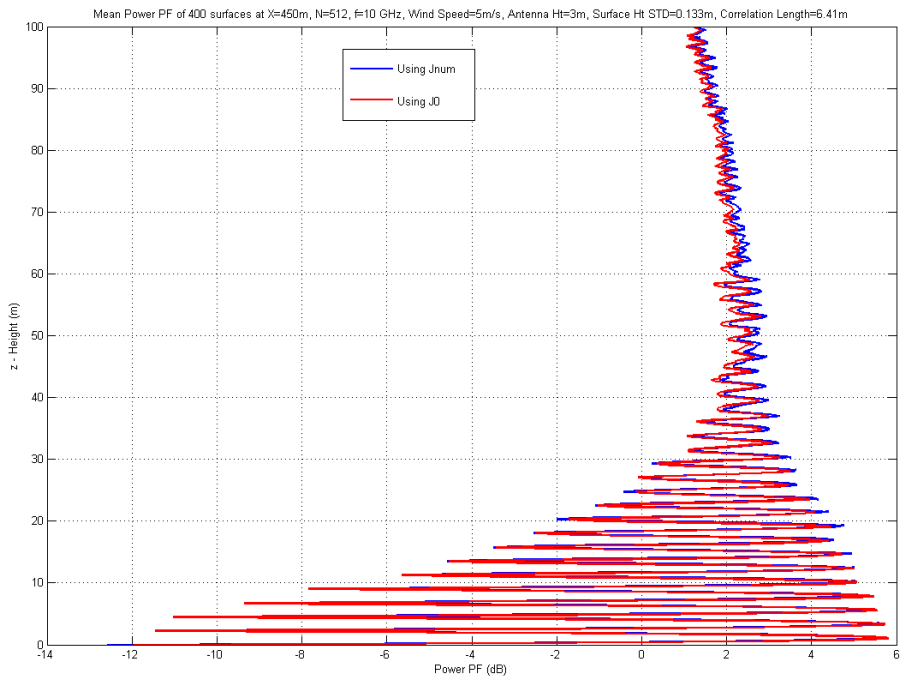


Figure 49: Monte-Carlo mean power PF of 400 surface realizations at 10 GHz, $\lambda=0.06\text{m}$, $H_t=3\text{m}$, $U=5\text{m/s}$, $\sigma_h=0.13\text{m}$, $\rho_c=6.41\text{m}$, $N_p=512$, $\Delta x=0.88\text{m}$, $X_{max}=450\text{m}$

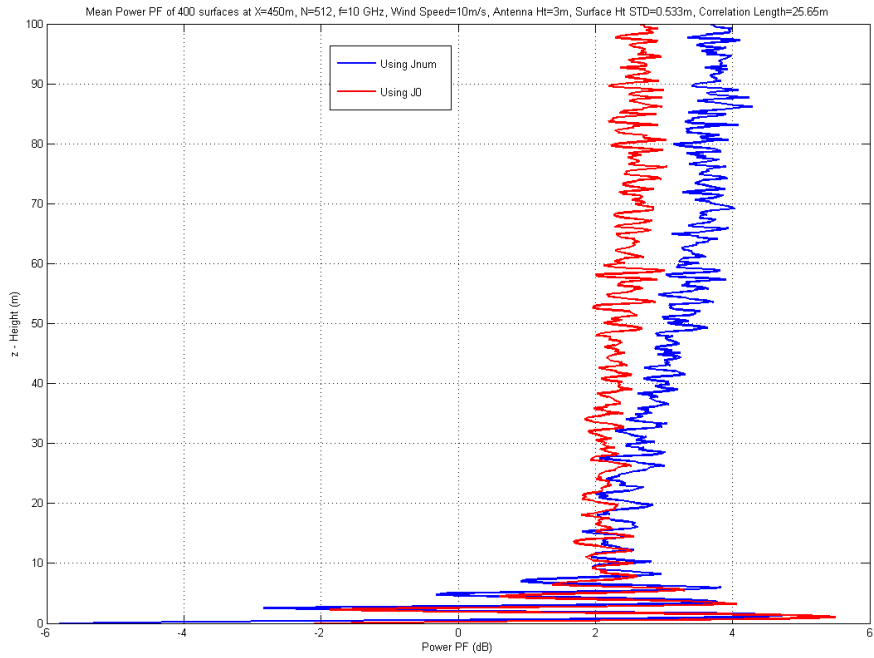


Figure 50: Monte-Carlo mean power PF of 400 surface realizations at 10 GHz, $\lambda=0.06\text{m}$, $H_f=3\text{m}$, $U=10\text{m/s}$, $\sigma_h=0.53\text{m}$, $\rho_c=25.6\text{m}$, $N_p=512$, $\Delta x=0.88\text{m}$, $X_{max}=450\text{m}$

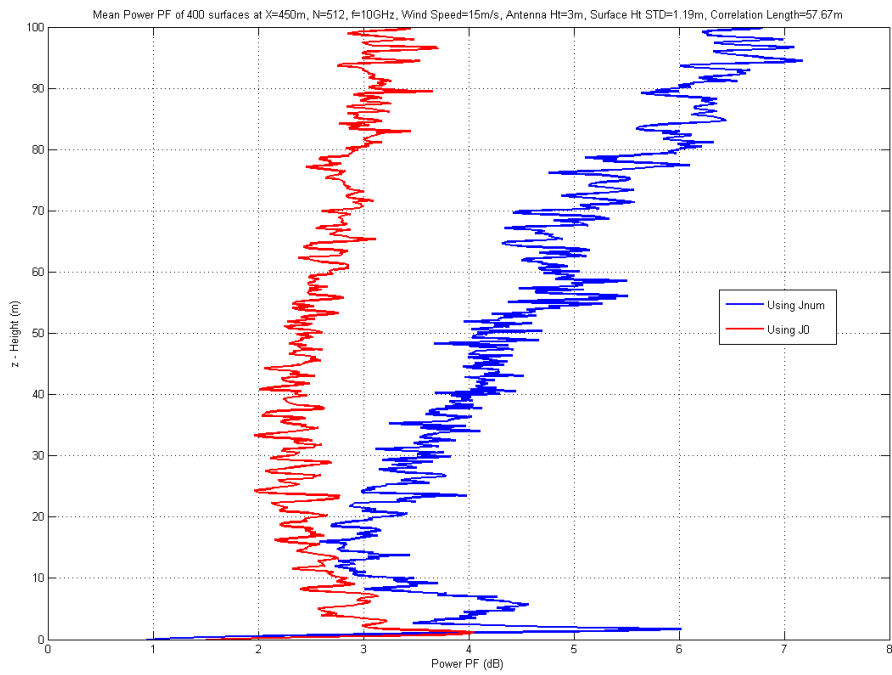


Figure 51: Monte-Carlo mean power PF of 400 surface realizations at 10 GHz, $\lambda=0.06\text{m}$, $H_f=3\text{m}$, $U=15\text{m/s}$, $\sigma_h=1.19\text{m}$, $\rho_c=57.73\text{m}$, $N_p=512$, $\Delta x=0.88\text{m}$, $X_{max}=450\text{m}$

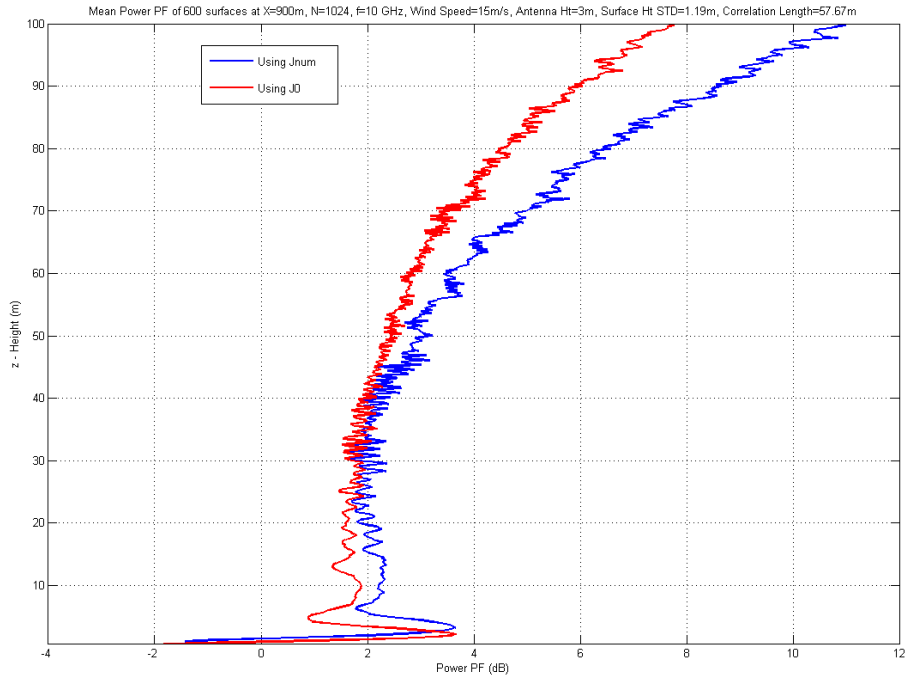


Figure 52: Monte-Carlo mean power PF of 400 surface realizations at 10 GHz, $\lambda=0.06\text{m}$, $H_t=3\text{m}$, $U=15\text{m/s}$, $\sigma_h=1.19\text{m}$, $\rho_c=57.73\text{m}$, $N_p=512$, $\Delta x=0.88\text{m}$, $X_{max}=900\text{m}$

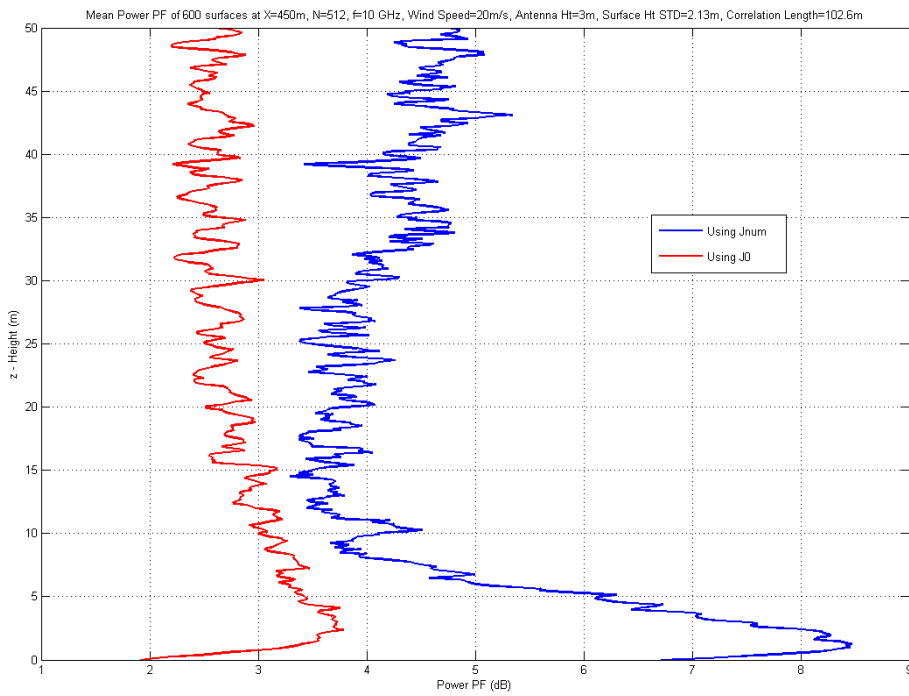


Figure 53: Monte-Carlo mean power PF of 400 surface realizations at 10 GHz, $\lambda=0.03\text{m}$, $H_t=3\text{m}$, $U=20\text{m/s}$, $\sigma_h=2.13\text{m}$, $\rho_c=102.6\text{m}$, $N_p=512$, $\Delta x=0.88\text{m}$, $X_{max}=450\text{m}$

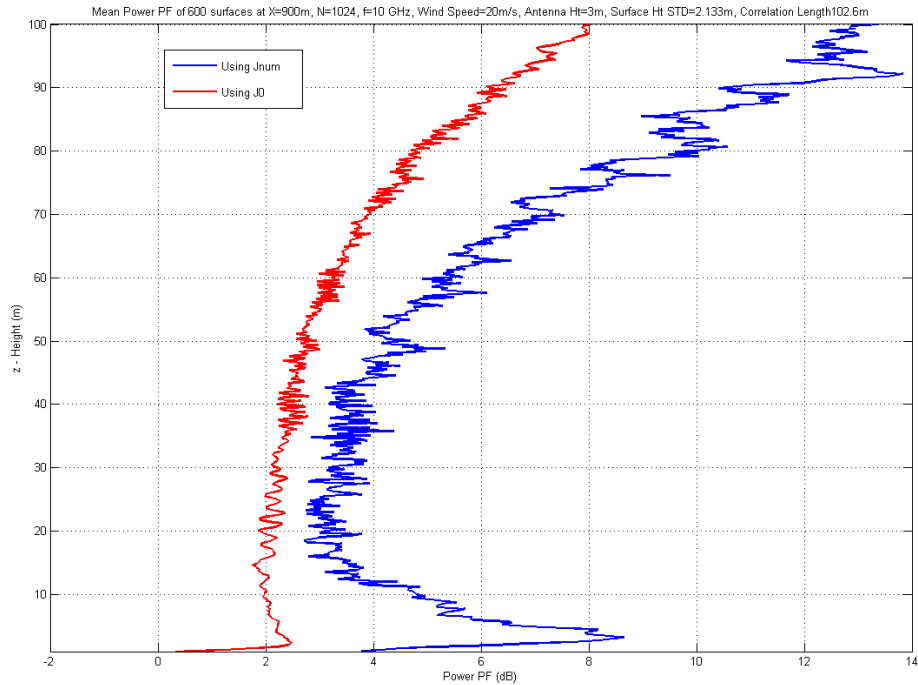


Figure 54: Monte-Carlo mean power PF of 400 surface realizations at 10 GHz, $\lambda=0.03\text{m}$, $H_r=3\text{m}$, $U=20\text{m/s}$, $\sigma_h=2.13\text{m}$, $\rho_c=102.6\text{m}$, $N_p=512$, $\Delta x=0.88\text{m}$, $X_{max}=900\text{m}$

It can be seen that the mean power PF breaks up and gets very noisy and unreliable at 10 GHz for the 15m/s and 20m/s cases (Fig. 51-54). We also see that the mismatch between Jnum and J0 is significantly large at 3 GHz (Fig. 44) and 5 GHz (Fig. 48) for the 20m/s case. These results are consistent with the validity exhibited in the mean signal PF plots and hence, the conclusion stands the same as before with the mean signal PF. Another observation is that the mean power PF generated using Jnum seems to increase and diverge more rapidly than J0. This may be attributed to the rest of the terms of Jnum other than zeroth order term contributing more significantly to the magnitude rather than the phase of the scattered field. As to why the mean non-coherent power PF does not converge to the incident power at large heights while the mean signal PF does converge, remains an open avenue to be investigated.

5.3. Asymptotic Zeroth Order Solution

Since the asymptotic zeroth order solution in Eq. 4.2.11 has good agreement with Ament, we consider analyzing its validity in each of the frequency bands. Due to its complex nature and 3D integral, its numerical computation can be laborious, but the cylindrical representation offers better numerical implementation than Cartesian coordinates. In order to obtain reasonably accurate results, the sampling along the ‘ ρ ’ domain is important and it is determined that in order to have a maximum phase difference of $\pi/4$ between successive points of the integrand, the step size in ‘ ρ ’ should be at least $\lambda/4z$, where maximum value of $z=100\text{m}$.

A representative speed i.e. 15m/s at each frequency is considered for comparison with the Monte-Carlo Jnum, Monte-Carlo J0, Miller-Brown, Ament and the results are shown below.

In each of the cases, the diffused field component $\langle \Delta U_s^0 \rangle$ is very small compared to the dominant $\langle U_s^1 \rangle$ term and hence the overall mean scattered field is not affected significantly.

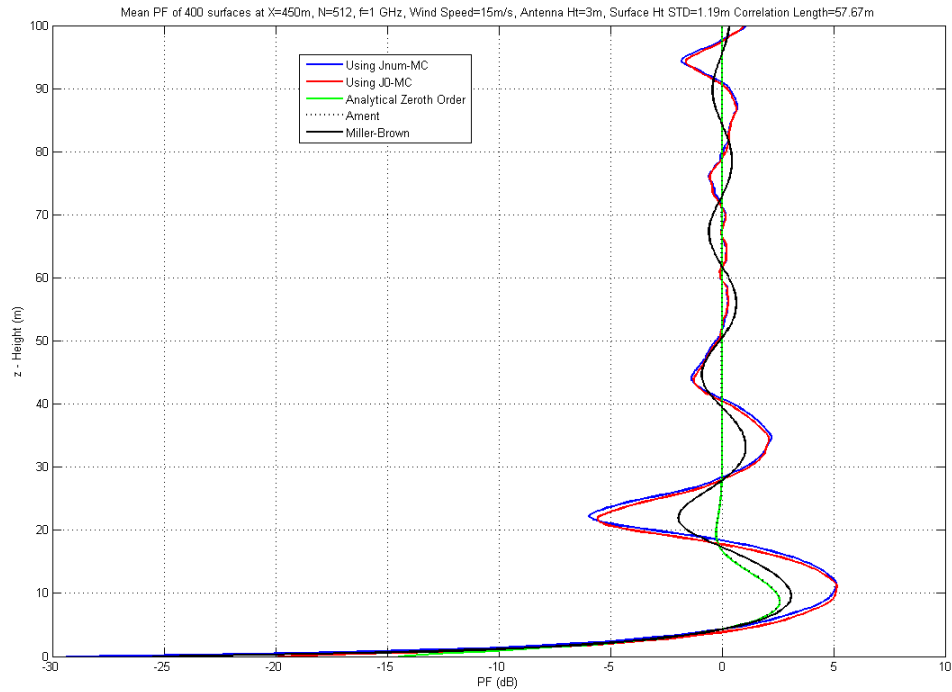


Figure 55: Comparison with asymptotic zeroth order at 1 GHz, $\lambda=0.3\text{m}$, $H_r=3\text{m}$, $U=15\text{m/s}$, $\sigma_h=1.19\text{m}$, $\rho_c=57.73\text{m}$, $N_p=512$, $\Delta x=0.88\text{m}$, $X_{max}=450\text{m}$

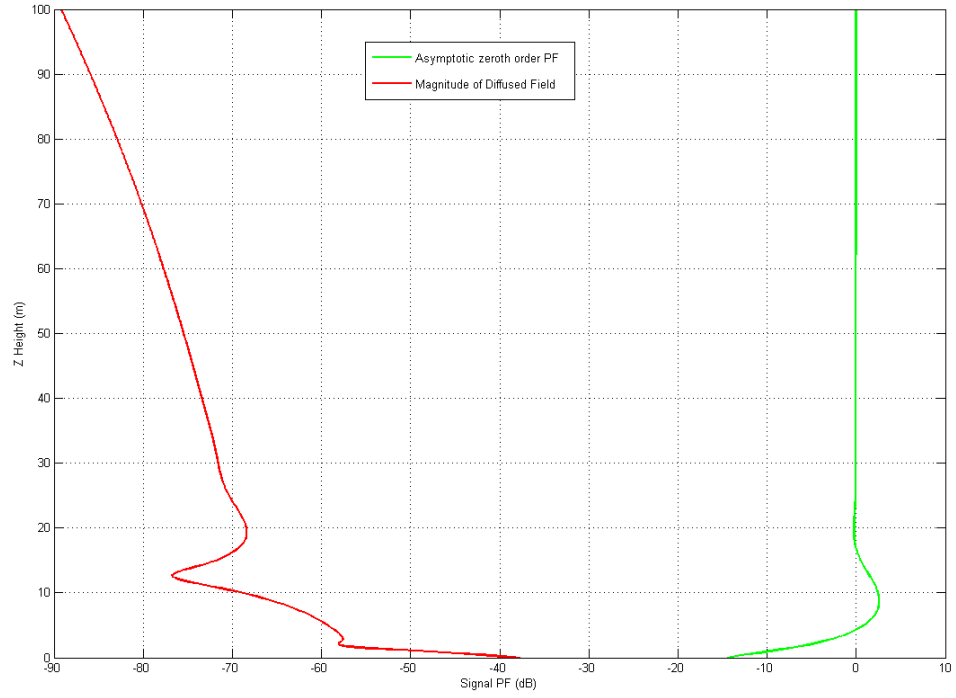


Figure 56: Diffused component of asymptotic zeroth order solution at 1 GHz, 15m/s

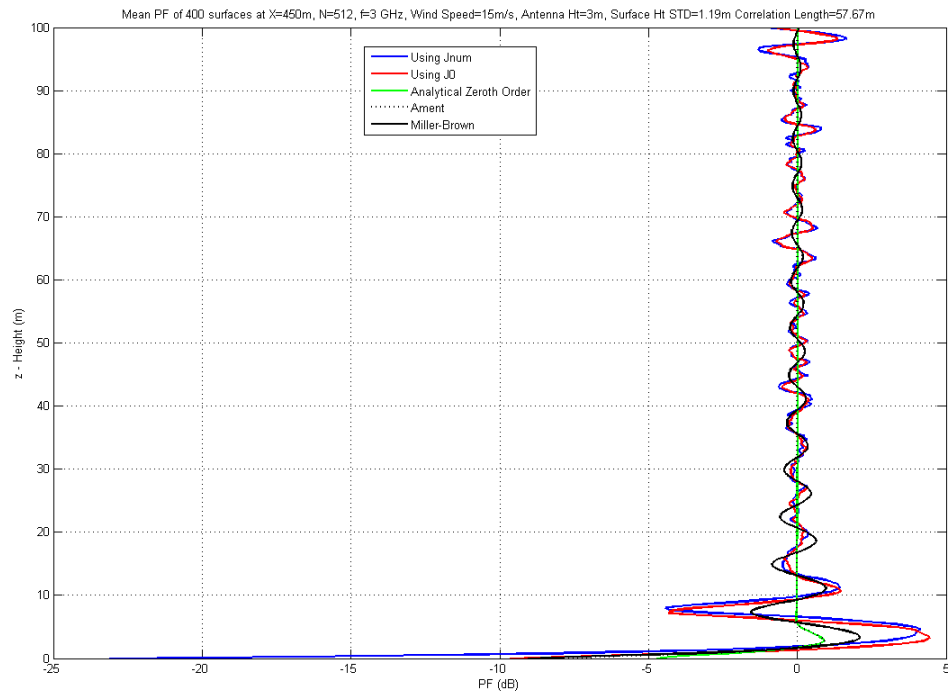


Figure 57: Comparison with asymptotic zeroth order at 3 GHz, $\lambda=0.1\text{m}$, $H_f=3\text{m}$, $U=15\text{m/s}$, $\sigma_h=1.19\text{m}$, $\rho_c=57.73\text{m}$, $N_p=512$, $\Delta x=0.88\text{m}$, $X_{max}=450\text{m}$

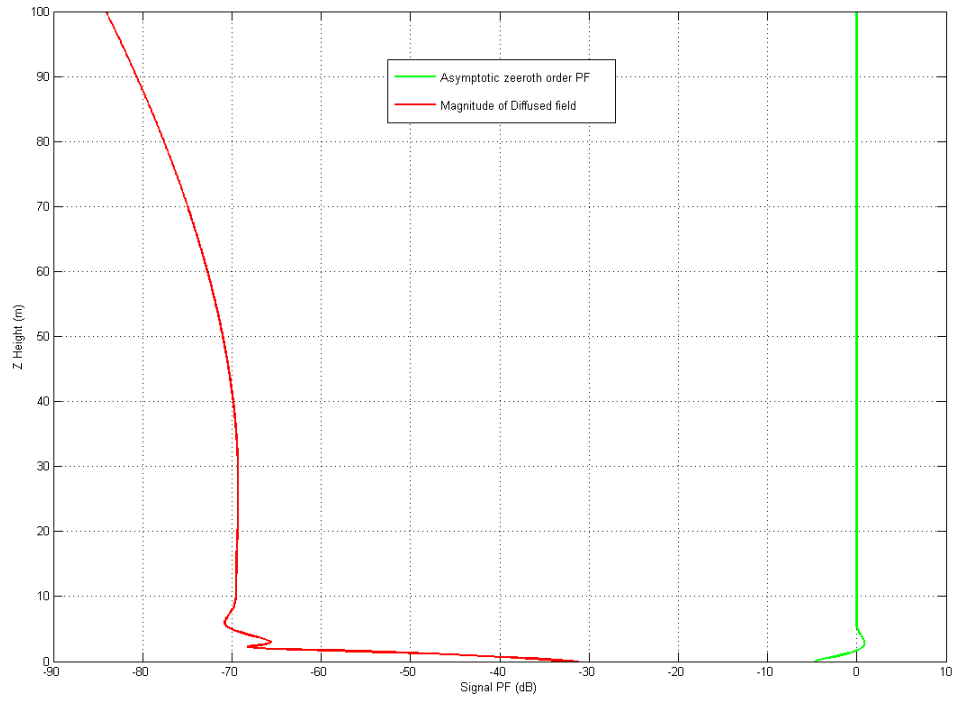


Figure 58: Diffused component of asymptotic zeroth order solution at 3 GHz, 15m/s

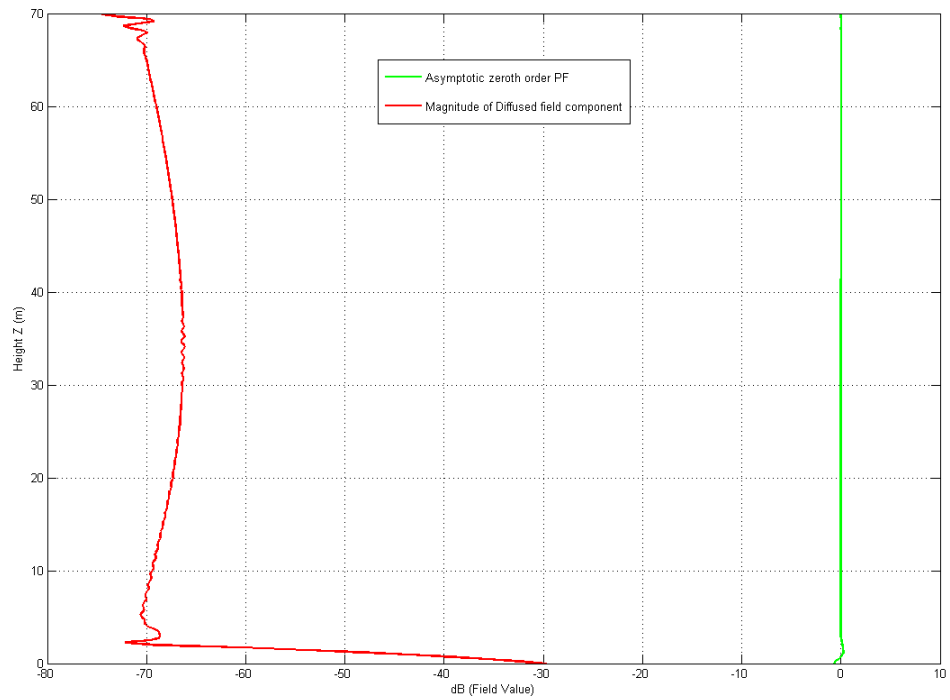


Figure 59: Diffused component of asymptotic zeroth order solution at 5 GHz, 15m/s

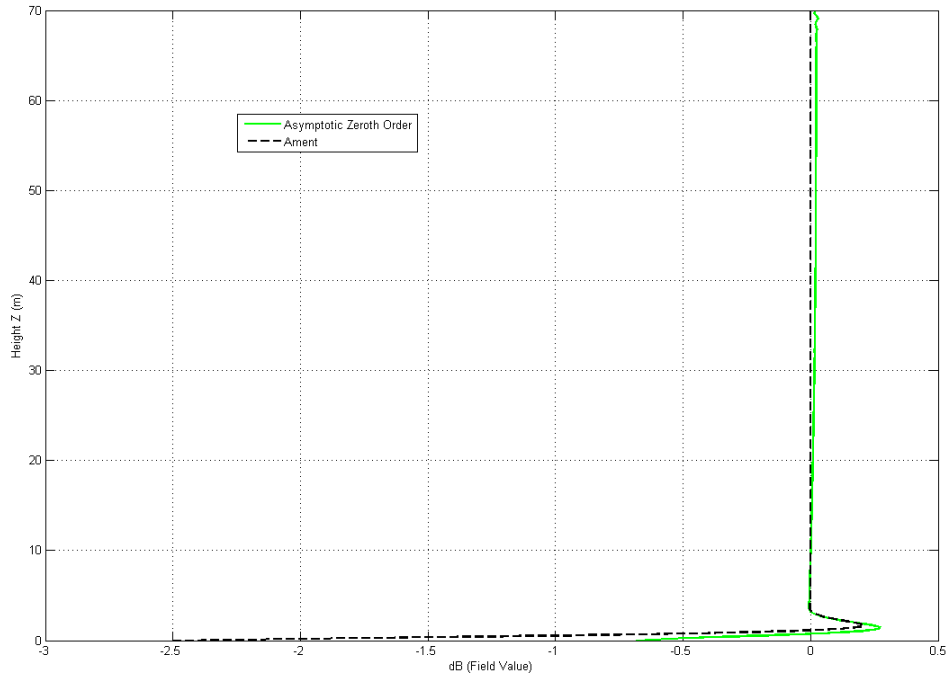


Figure 60: Comparison of asymptotic zeroth order solution at 5 GHz, 15m/s with Ament

We can observe that the diffused component increases slightly with frequency, but is at least 40 dB down from the dominant specular component and hence, does not significantly impact the overall mean PF. The diffused component exhibits higher magnitude closer to the surface since the multiple non-specular reflections and diffractions are dominant closer to the surface. At 10 GHz, the resolution along the ρ domain for accurate results in diffused component requires to be about $\Delta\rho = 7.5 \times 10^{-5}$, which results about 30,000 points for the 3D integral computation. This gets quite cumbersome for computation and the resulting mean PF is quite noisy. Hence, we represent our analysis up to 5 GHz.

CHAPTER 6

Summary and Conclusions

Although there is extensive literature on theoretical and numerical techniques for the rough surface scattering problem, there is relatively little work done on the analysis of the zeroth order solution (both Monte-Carlo and analytical), which is the core component of this thesis. Predicting the mean propagation factor using the exact solution to current density and comparing it with zeroth order solution is an integral part of the work. Scattering of electromagnetic waves from one-dimensional perfectly conducting large rough surfaces at low grazing angles is considered. Since, the Monte-Carlo simulation for large rough surfaces requires significant computational time investment; an asymptotic solution based on the zeroth order current density is formulated and compared with the numerical techniques. Both the mean coherent and non-coherent propagation factors i.e. signal and power respectively were computed and analyzed for the scope of the zeroth order solution. In all numerical simulations, the surface height is assumed to have a Gaussian probability density function and the surface spectra to be the ocean-like Pierson-Moskowitz spectrum, although the current technique would work just fine for the Gaussian spectrum, periodic surfaces like the sine surface and other partially developed sea-spectra.

Based on a subjective quantitative analysis of the phase mismatch between the exact and zeroth order solutions, it is predicted that mean Monte-Carlo simulation using the Volterra integral equation of the second kind is reasonably accurate up to about RMS surface height equal to 20 wavelengths of the incident electromagnetic wave and a normalized mean phase error < 1 degree relative to the number of nulls which are 3 dB below incident field. The cause of noisy pattern at certain frequencies and wind-speeds may be attributed to the following reasons:

1. Since the Monte-Carlo solution error convergence rate is inversely proportional to the square root of number of realizations, the current number of realizations (i.e. 400 surfaces) may not be adequate.

2. Limitations on the accuracy of number of significant digits that can be processed by the software (i.e. Matlab in this case) running the computation.
3. The diffused components of the scattered field are significantly high that any meaningful interference pattern cannot be visualized.

The diffused component corresponding to the non-specular reflection terms of the asymptotic zeroth order solution is significantly smaller compared to the dominant specular reflection term. Although the results shown are limited to 450m horizontal range, the grazing angles reduce at farther distances and hence the accuracy of the solutions would be slightly better. Increasing sampling resolution on the rough surface seems to have little effect on improving the zeroth order accuracy.

The thesis can be summarized as follows. Chapter 1 presents an introduction to the thesis, the necessary technical background and motivation to pursue such a topic of interest. Chapter 2 explains the essential steps for modeling a random rough surface based on signal-processing concepts and probability distribution of random variables. Chapter 3 describes the integral equations and their derivation for computing the induced current densities based on PE approximation and Green's function and its properties. This results in a new Volterra integral equation of the second kind which is solved exactly without any matrix inversion ^[1]. The chapter entails the expressions for the first term of the infinite series solution known as the zeroth order solution.

Chapter 4 presents the steps required to compute the scattered field along a vertical line. This process involves discretizing the Volterra integral equation, expressing it as a sum of sub-integrals and applying a linear approximation to the current densities and surface profile to result in expressing each sub-integral in terms of Fresnel integrals, which are numerically feasible and attractive technique to solve for the scattered field. The chapter also demonstrates the use of an analytical expression for the asymptotic zeroth order solution that saves the time required in case of Monte-Carlo simulations. Analysis of specular and non-specular reflection is done to compare existing techniques with the new methodology.

Chapter 5 illustrates and analyzes the validity of the zeroth order solution in terms of both Monte-Carlo simulations and asymptotic expressions. A quantitative analysis is done to predict the scope and bound of the zeroth order solution at varying frequencies and surface roughness.

Core contributions of this thesis are as follows:

- Mean propagation factor prediction and computation using Monte-Carlo simulations based on a novel Volterra integral equation of the second kind ^[1] and analysis of zeroth order solution
- Analysis and computation of an analytical asymptotic zeroth order solution ^[11] for the mean propagation factor resulting in significantly less time investment compared to Monte-Carlo simulations
- Investigation of the scope and validity of the Monte-Carlo simulations and analytical solutions at varying frequencies and surface roughness parameters based on quantitative analysis
- Mean non-coherent power propagation prediction using Monte-Carlo simulations and comparison with a known analytical approach

It is hoped that the analytical expression based on the asymptotic zeroth order solution will be useful in propagation modeling for radar detection and in wireless communication. One future scope of this work would be to extend the methodology to surface modeled by impedance boundary conditions and to 3-D propagation over 2-D rough surfaces.

BIBLIOGRAPHY

- [1] J.G. de Boer. "On the Correlation Functions in Time and Space of Wind-Generated Ocean Waves", *Technical Report No.160*, Saclant ASW Research Center (Dec 1969).
- [2] Axline R M and Fung A K, "Numerical computations of scattering from a perfectly conducting random surface", *IEEE Transactions on Antennas & Propagation*, Vol. 26, pp. 482–488
- [3] Garcia N and Stoll E, "Monte Carlo calculation for electromagnetic-wave scattering from random rough surfaces" *Phys. Revision Letter*. 52 pp. 1798–1801, (1984)
- [4] Pak K, Tsang L and Chan C H, "Backscattering enhancement of electromagnetic waves from two-dimensional perfectly conducting random rough surfaces based on Monte Carlo method", *J. Opt. Soc. Am. A*, 12, pp. 2491–2499 (1995)
- [5] Marchand R T and Brown G S, "On the use of finite surfaces in the numerical prediction of rough surface scattering" *IEEE Trans. Antennas & Propagation*, Vol. 47, pp. 600–604 (1999)
- [6] Karl F Warnick and Weng Cho Chew, "Numerical Simulation Methods for Rough Surface Scattering", *Waves in Random Media*, 11:1, R1-R30, (2001)
- [7] R. Janaswamy. "Direct Solution of Current Density Induced on a Rough Surface by Forward Propagating Waves", *IEEE Transactions On Antennas and Propagation*, (July 2013), Vol. 61, No. 7.
- [8] Z. Lai. "Electromagnetic Wave Propagation over Large Rough Surfaces at Low Grazing Angles", *Ph.D. Dissertation*, University of Massachusetts Amherst, MA (Sep 2007).
- [9] D. E. Freund, N. E. Woods, H.C. Ku, and R. S. Awadallah. "Forward Radar Propagation Over a Rough Sea Surface: A Numerical Assessment of the Miller-Brown Approximation Using a Horizontally Polarized 3-GHz Line Source", *IEEE Transactions on Antennas and Propagation*, Vol. 54, No. 4, (April 2006).

- [10] W. S. Ament. "Toward a Theory of Reflection by a Rough Surface", *Proceedings of the I.R.E*, pp. 142-146, (Oct 1952).
- [11] R. Janaswamy, Unpublished notes on the derivation of zeroth order asymptotic expressions for the mean scattered field
- [12] E. I. Thorsos, "Acoustic scattering from a "Pierson-Moskowitz" sea surface," *J. Acoust. Soc. Amer.*, vol. 88, no. 1, pp. 335–349, Jul. 1990
- [13] R. Janaswamy. "Radiowave Propagation and Smart Antennas for Wireless Communications", Kluwer Academic Publishers, pp. 279-285.
- [14] M.J. de Assis Motta. "Equivalent Impedance of Rough Surface at Low Grazing Angles", *M.S. Thesis*, Naval Postgraduate School, Monterey, CA, (Sep 1999).
- [15] I. Sirkova. "Propagation Factor and Path Loss Simulation Results for Two Rough Surface Reflection Coefficients Applied to the Microwave Ducting Propagation over the Sea", *Progress In Electromagnetics Research M*, Vol. 17, 151-166, (2011)
- [16] P. Beckmann and A. Spizzichino, "The Scattering of Electromagnetic Waves from Rough Surfaces" New York, NY, USA: Pergamon, (1963).
- [17] Z. Lai and R. Janaswamy. "Specular Propagation over Rough Surfaces: Numerical Assessment of Uscinski and Stanek's Mean Green's function technique", *Waves in Random and Complex Media*, Vol. 16, No. 2, pp. 137-150, (May 2006).
- [18] Rayleigh, J. W. S., "The Theory of Sound", Dover Publications, Inc., New York (1945).